

Volcanism and geochemistry of the Kamloops Group, south-central British Columbia



Van Wagoner, N.¹, Ootes, L.², and Thomson-Gladish, J.^{1,3}

¹Thompson Rivers University, Department of Earth Sciences, Kamloops, BC, V2C 0C8

²British Columbia Geological Survey, Ministry of Energy, Mines and Low Carbon Innovation, Victoria, BC, V8W 9N3

³Archer, Cathro & Associates (1981) Limited, 1016-510 West Hastings Street, Vancouver, BC, V6B 1L8

^acorresponding author: Luke.Ootes@gov.bc.ca

Recommended citation: Van Wagoner, N., Ootes, L., and Thomson-Gladish, J., 2021. Volcanism and geochemistry of the Kamloops Group, south-central British Columbia. In: *Geological Fieldwork 2020*, British Columbia Ministry of Energy, Mines and Low Carbon Innovation, British Columbia Geological Survey Paper 2021-01, pp. 65-88.

Abstract

The Challis-Kamloops belt (early Eocene) includes graben-fill volcanic and sedimentary rocks that extend for about 2000 km from Challis in Idaho to central British Columbia and possibly, into southern Yukon. Mapping and sampling of the Kamloops Group in the south-central part of the belt indicates subaerial to subaqueous (lacustrine) volcanism, with volcanic facies in the type area including mega pillows, hyaloclastites, pahoehoe and aa flows, domes and phreatomagmatic cones. New geochemical data indicate that the rocks are calc-alkaline to weakly alkaline basaltic andesite to trachy-andesite, with adakitic characteristics. The major element compositions are influenced primarily by fractionation of pyroxene and olivine. The chondrite-normalized REE patterns are uniform and LREE-enriched, with relatively flat HREE patterns. The rocks have primitive mantle-normalized trace element patterns that are arc-like with positive LILE and negative HFSE anomalies. A preliminary comparison of Kamloops Group geochemistry (new and previously published data), and published data from other Eocene units (Princeton and Pentiction groups) of the Challis-Kamloops belt in south-central British Columbia indicates distinct geographic differences. The Kamloops and Princeton group melts may have been derived from the spinel-garnet transition zone in the subcontinental lithospheric mantle and influenced by slab-derived fluids, whereas the Pentiction Group shows trends toward anhydrous enrichment and may have been derived from a different source. Among the three groups there is a lateral decrease in Ba/La from west to east reflecting a declining intensity of slab-derived fluids from an Eocene subducting margin.

Keywords: Eocene, Kamloops Group, volcanic rocks, physical volcanology, geochemistry

1. Introduction

The Challis-Kamloops belt (Eocene) is a narrow (<200 km) discontinuous belt of graben-fill volcanic and sedimentary rocks that extends for about 2000 km from the Challis volcanic field in Idaho through central British Columbia and possibly as far north as southern Yukon (e.g., Dostal et al., 2001, 2003, 2019; Bordet et al., 2014). In different parts of British Columbia these rocks have been referred to by different group-level names (Fig. 1; Kamloops, Pentiction, Princeton, Ootsa Lake, Endako, Nechako Plateau, and Sloko); in southwest Yukon, the term Skukum volcanic complex is used (e.g., Morris and Creaser, 2003). Magmatism in the belt continued from ca. 56 Ma (Ypresian) to ca. 47 Ma (Lutetian; e.g., Love et al., 1998; Bordet et al., 2014). Mineralization spatially and/or temporally associated with this magmatism includes local occurrences of porphyry Cu-Mo, epithermal-Au, coal, concentrations of REE, zeolite deposits, and aggregate (e.g., Love et al., 1998). The volcanism coincides with the Early Eocene Climatic Optimum (Smith et al., 2010; Zachos et al., 2001, 2008) and may have affected local if not regional to global climate.

The present study is part of a province-wide investigation of the Challis-Kamloops belt intended to better understand the drivers of Eocene volcanism and the relationships between

volcanism, mineralization, and climate. We focus on the Kamloops Group, in the interior of south-central British Columbia (Fig. 1). Previous studies indicated that Kamloops Group volcanic rocks are mostly subaerial and lacustrine basalt to andesite flows, with lesser felsic volcanic and sedimentary rocks (Ewing, 1981a, b, c and 1982; Breitsprecher, 2002; Breitsprecher et al., 2003). Herein we present the preliminary results of mapping and sampling to more fully document the physical volcanology and geochemistry of the Kamloops Group in its type area, and to compare the geochemistry of the Kamloops Group to that of the Princeton and Pentiction groups nearby.

2. Setting and previous work

Magmatism in the Challis-Kamloops belt was during northeast-southwest extension of the Cordilleran orogen, which resulted in the generation of semi-isolated grabens that accumulated sedimentary and volcanic rocks (e.g., Ickert et al., 2009). Various drivers have been suggested for the volcanism, including normal arc volcanism (Morris and Creaser, 2003), subduction angle migration and plate rotation (Haeussler et al., 2003), magmatism related to a slab-tear (Breitsprecher et al., 2003; Dostal et al., 2001, 2003, 2008, 2019; Madsen et al.,

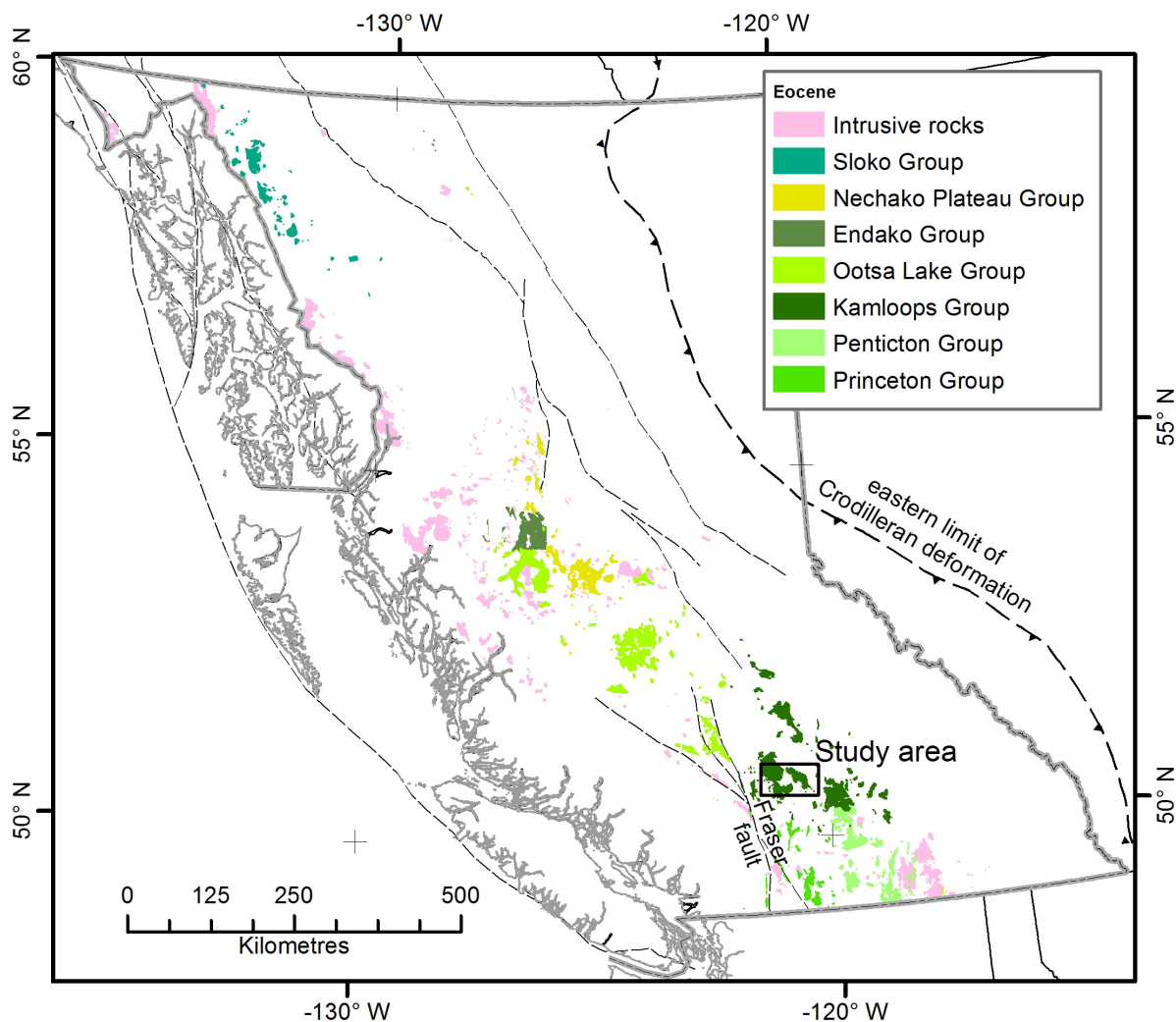


Fig. 1. Distribution of Eocene (ca. 56 to 47 Ma; Ypresian to Lutetian) volcanic and intrusive rocks of the Challis-Kamloops belt in British Columbia and location of study area. Grey dashed lines are Eocene dextral strike-slip faults.

2006; Ickert et al., 2009), plume-induced subduction initiation (Stern and Dumitru, 2019), and subduction termination and development of a slab gap (Bordet et al., 2014).

The Kamloops Group is an assemblage of Ypresian (ca. 52 Ma) volcanic and lesser sedimentary rocks exposed from between Cache Creek eastward to Kamloops and extending 5-10 km to the north and south (Fig. 2). The rocks mostly overlie Mesozoic basement of the Quesnel terrane with some in the east overlying North American basement. The Fraser fault (dextral strike slip) separates the Kamloops Group from the Ootsa Lake and Endako groups to the northwest (Fig. 1; e.g., Dostal et al., 2001; Bordet et al., 2014). As will be discussed further below (section 5.3.), the boundary between the Kamloops Group and the Princeton and Pentiction groups is arbitrary.

The most comprehensive studies of the Kamloops Group were by Ewing (1981a, b, c; 1982) and Breitsprecher (2002). Ewing (1981a, b, 1982) divided the Kamloops Group in its type area into the Tranquille Formation comprising the Border facies and the informal upper, middle, and lower members and the

overlying Dewdrop Formation, subdivided into nine informal members (Fig. 3). Ewing (1982) produced a 1:50,000-scale map of the type area. Ewing (1981a, b) also contributed more detailed maps of the Savona area and the McAbee fossil beds (Tranquille Formation), a British Columbia Heritage site. Breitsprecher (2002) completed local mapping in eastern exposures of the Kamloops Group and, along with Dostal et al. (2019) contributed geochemical data.

Previous mapping indicated that the Tranquille Formation comprises lacustrine to deltaic coarse arkosic-lithic wackes (Border facies), shale, tuffaceous siltstone, and tuffs that are interbedded with flows, pillowed flows and hyaloclastites (Ewing, 1981a, b; 1982). The McAbee fossil beds, included within the Tranquille Formation, contain abundant flora and fauna (e.g., Smith et al., 2010; Greenwood et al., 2005; Lowe et al., 2018a, b; Mayr et al., 2019) and have been included in the Okanagan Highlands *Lagerstätten* (Archibald et al., 2011). This *Lagerstätten*, is significant because it provides a record of the paleoecology and climate of the region during the Early

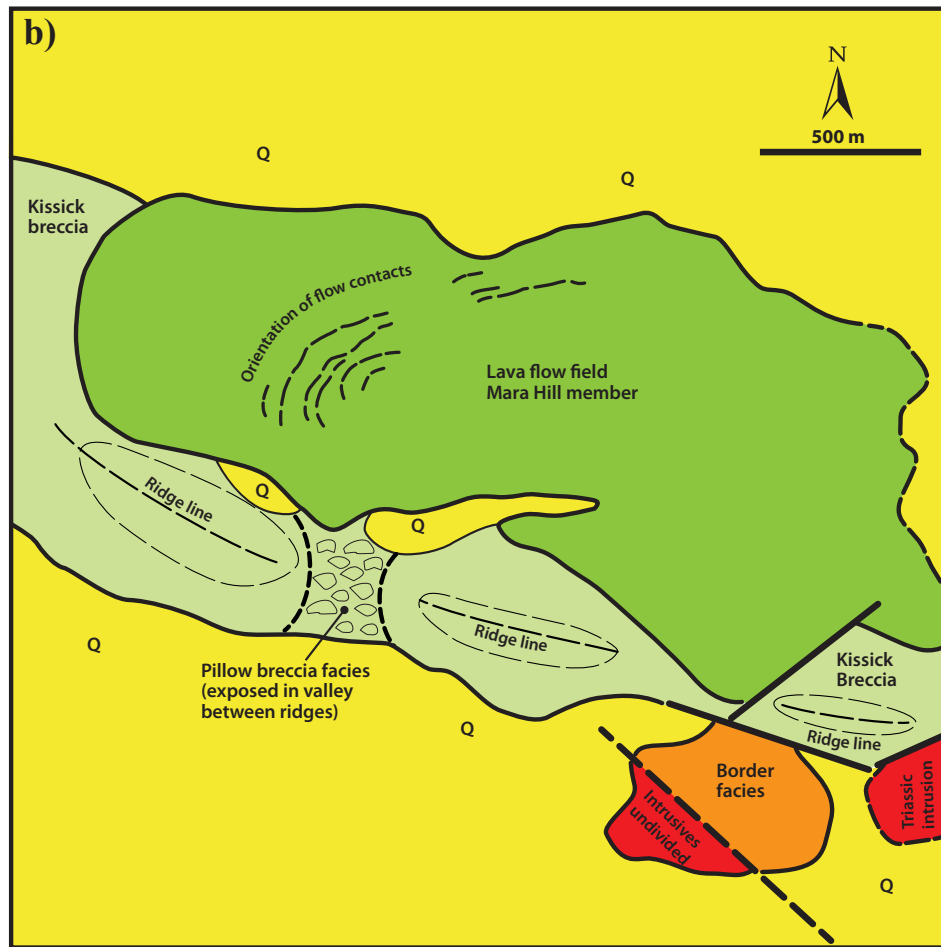
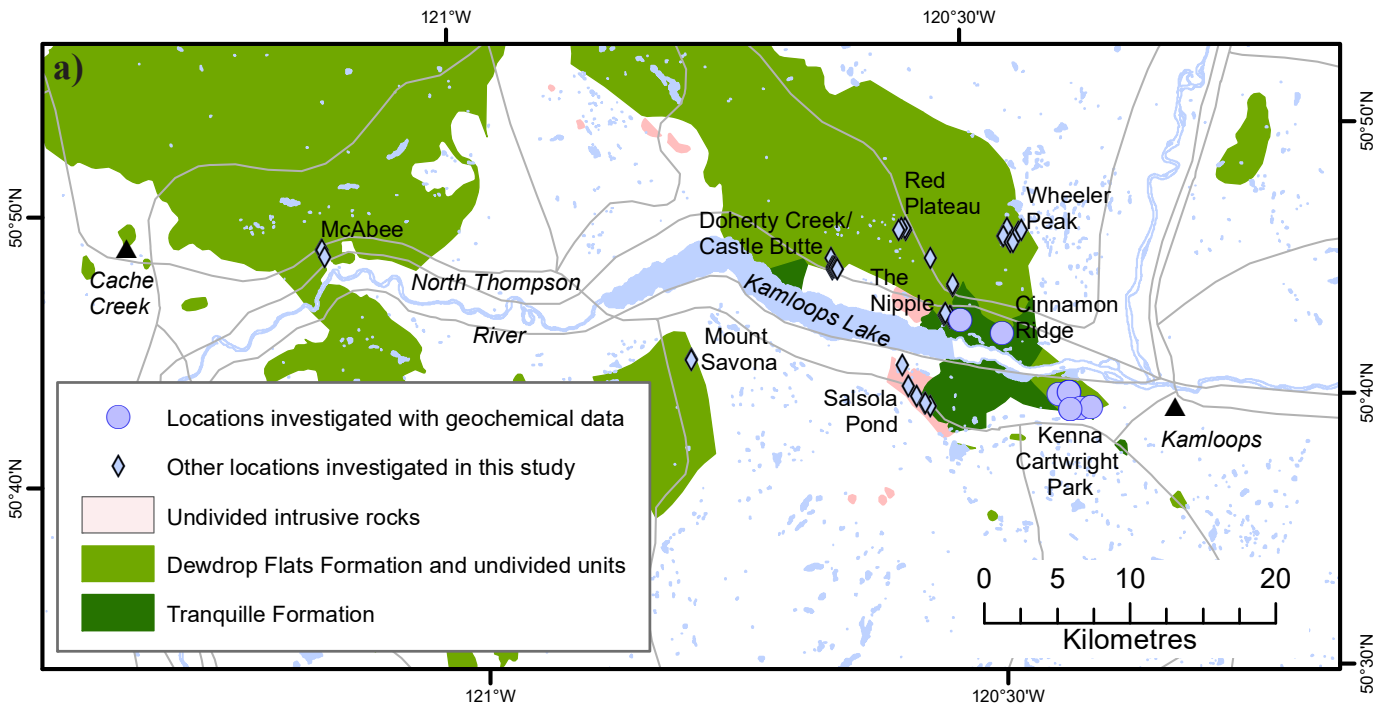


Fig. 2. a) Distribution of volcanic and intrusive rocks of the Kamloops Group, west of the City of Kamloops. Blue circles are locations examined in 2019 with geochemical data presented herein. Blue diamonds are locations examined in 2020. **b)** Sketch map of Kenna Cartwright Park showing the distribution of different rock units and topographic features. Q – Quaternary sediments. Modified from Ewing (1982).

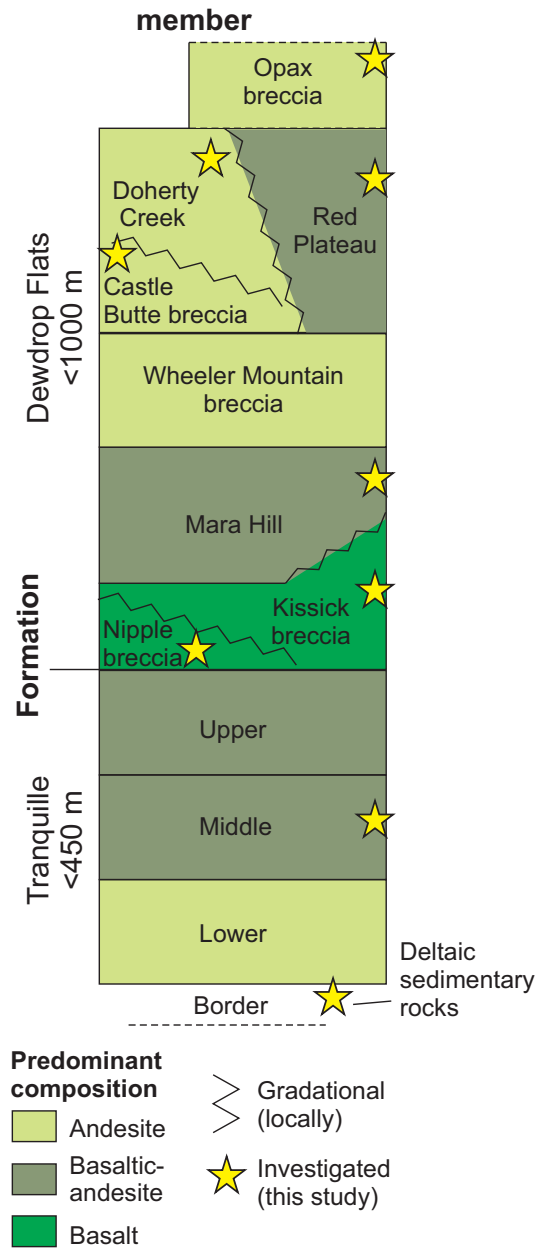


Fig. 3. Generalized stratigraphy of the Kamloops Group (simplified after Ewing, 1981a).

Eocene Climactic Optimum (Archibald et al., 2011; Greenwood et al., 2016; West et al., 2020). Ewing (1981a, b) correlated the McAbee beds to the “upper unit” of the Tranquille Formation based on their similar rock types. These beds were since ascribed to an unnamed member of the Tranquille Formation (Read and Hebda, 2009). The Dewdrop Formation is predominantly basaltic to andesitic sub-lacustrine to subaerial flows, flow breccias, cones, tuff rings and a composite cone (Ewing, 1981a, 1982).

3. Field investigations of physical volcanology

The map and field descriptions of the type area of the

Kamloops Group by Ewing (1981a, b, 1982) were used as a basis for this sampling program. In general, the rocks are well exposed in much of the area, and primary structures are well preserved, but units are laterally discontinuous and informal members of the Tranquille and Dewdrop formations include a variety of volcanic facies. The coherent flows and intrusions tend to be more resistant than the fragmental units, which tend to be more recessive and form soil-covered slopes. With the exception of volcanic glasses that have been altered to palagonite, alteration is minimal. Our sampling focussed on two parts of the Kamloops Group type area, Kenna Cartwright Park, which is underlain by the Border facies of the Tranquille Formation and the Mara Hill and Kissick members of the Dewdrop Flats Formation, and Cinnamon Ridge exposures of the middle member of the Tranquille Formation. We also examined rocks of the Kamloops Group at the Nipple, Doherty Creek/Castle Butte, Red Plateau, Wheeler Peak, Mount Savona, and McAbee localities (Fig. 2).

3.1. Kenna Cartwright Park

3.1.1. The Lava flow field; Mara Hill member, Dewdrop Flats Formation

The portion of Kenna Cartwright Park mapped by Ewing as the Mara Hill member of the Dewdrop Flats Formation (Figs. 2, 3; Ewing, 1981a, 1982) comprises a section of stacked subaerial pahoehoe flows about 210 m thick covering an area of about 2.5 km². These flows are overlain by Quaternary sediments to the north and interfinger with monolithic basaltic breccias of the Kissick member to the south (Fig. 2b). Individual flows are 1.5 to 3 m thick, but pahoehoe toes are as thin as few cm to 10 to 20 cm, with glassy chill margins 1 to 5 cm thick (Fig. 4a). Flows are aphyric to sparsely plagioclase phyric and are sparsely vesicular (ca. 5%), with flow-aligned vesicles (2-4 cm long), and vesicle trails at the lower third of some of the thicker flows. However, some flow tops and individual flows are highly vesicular (20-30%) with spherical vesicles up to 3-4 cm in diameter. Flow features are remarkably well preserved and include small tumuli, lava tubes, pahoehoe toes, and ropy pahoehoe surfaces (Fig. 4). The concentration of these features at the top of the sequence may indicate a decline in the lava supply rate and transition to tube-fed flows (e.g., Anderson et al., 2012), or be a function of exposure.

Other lava flows are south of the Lava flow field and separated from it by outcrops of Kissick breccia and a west-northwest trending fault. Ewing (1981a) considered these flows as possibly being part of the Border facies, the unit at the base of the Tranquille Formation (Figs. 2b, 3). These lava flows are aphyric, to sparsely pyroxene and plagioclase microphyric, and massive to sparsely vesicular.

3.1.2. Kissick breccia member andesitic breccias, Dewdrop Flats Formation

The Kissick breccia member of the Dewdrop Flats Formation (Ewing, 1981a, 1982) forms an east-west trending ridge south of, and in contact with, the Lava flow field (Fig. 2b), where

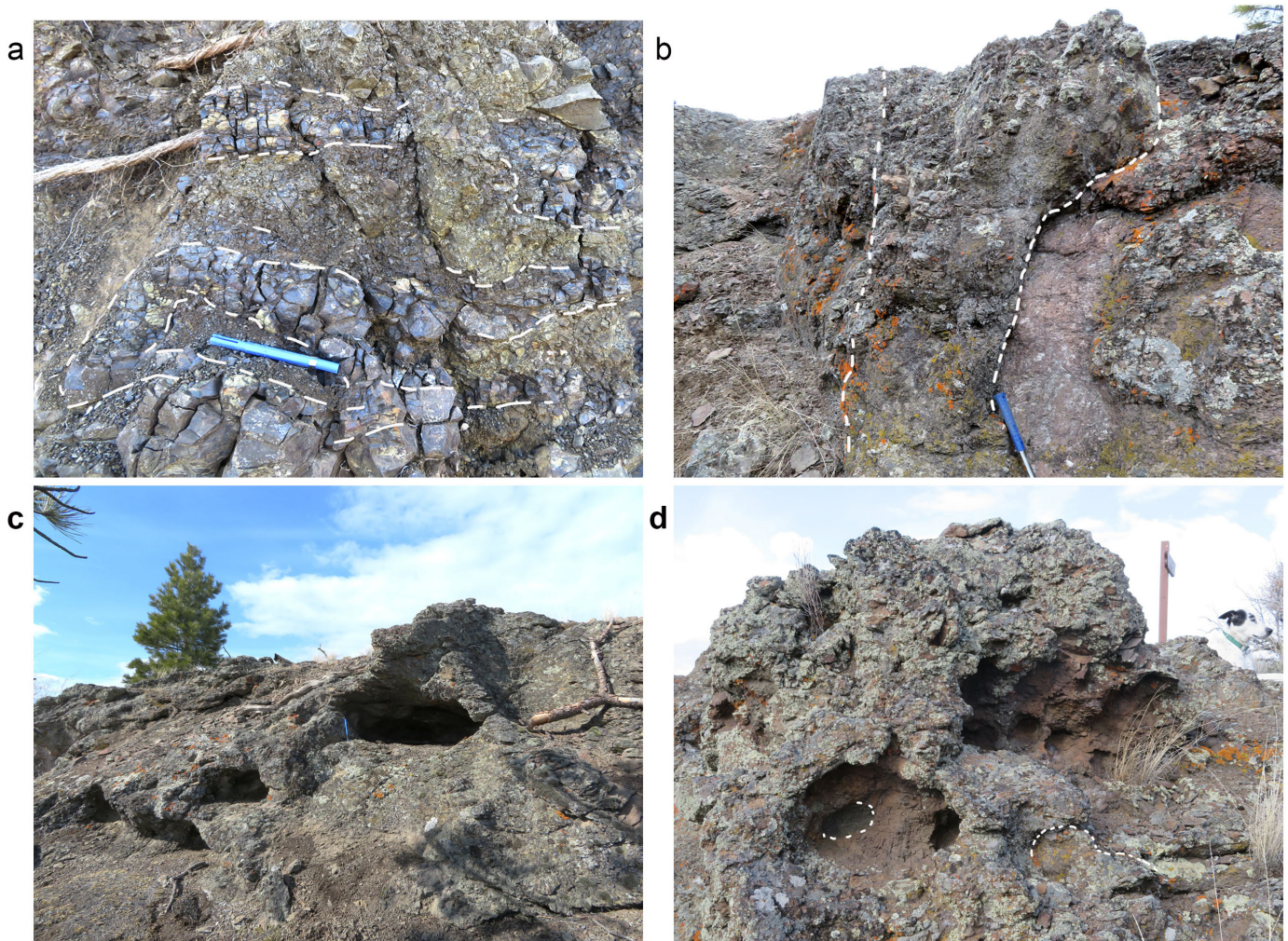


Fig. 4. Kenna Cartwright Park, flow features of the Lava flow field (the Mara Hill member, Dewdrop Flats Formation. **a**) Thin pahoehoe toes with vitric margins (outlined) and aphanitic interiors. The eraser tube, set inside one of the pahoehoe toes, is 13 cm long. **b**) Synvolcanic dike, or squeeze-up through a lava flow. Hammer handle is 28 cm. **c**) Drain-away tubes with a small tumulus at the top of a thick pahoehoe flow. **d**) Intermingling flow toes showing drain-away features; a budding tube or toe on the right and a filled tube inside of a larger cavity on the left. The cavity on the lower left is about 30 cm in diameter.

andesitic breccias occur stratigraphically above and below the flows. All of the breccias are monolithic but they differ in terms of volcanic structures and textures.

Where the breccia is beneath the lava flows (Fig. 2b) it is a monolithic pillow breccia, comprising bulbous pillow forms up to 40 cm (Figs. 5a-c) with partial chill margins that are brecciated such that fragments are only slightly separated and display a jig-saw fit. These broken pillow forms are mixed with a hyaloclastite of more blocky fragments ranging from a few mm to about 30 cm that appear to have been remobilized during and following fracturing (Figs. 5b, c). The breccias are clast-supported with a matrix of finer, mostly angular fragments. Beds, 0.5-1 m thick, display vague bedding defined by the alignment of elongate larger broken to more intact pillow fragments (Fig. 5a), with primary dips of about 20°. We interpret these breccias immediately beneath the Lava flow field constitute a lava-fed lacustrine delta, primarily on the

basis of the elongation and fracturing of some of the pillow-like forms, depositional dips, mix of remobilized and jig-saw fit breccias, and general similarity with deposits that have been described elsewhere (Skilling, 2002). The combination of in-situ brecciation, as indicated by the jig-saw fit of some clasts, and chaotic fragmentation and beds with primary dips suggests deposition at the topset to foreset transition. Conceivably, flows from the immediately overlying part of the Lava flow field prograded over these breccias.

Breccias above the Lava flow field at higher elevations on the ridge, are a monolithic mix of agglutinate (appearing to be deposits of more plastic ejecta) along with more angular breccias. Overall, this andesitic breccia is sparsely vesicular and aphyric, or sparsely plagioclase phyrlic. The breccias are massive, clast supported and poorly sorted with clast size ranging from 1 to 2 m in diameter down to coarse ash. Locally, hackly fractured lava bodies are surrounded by more coherent

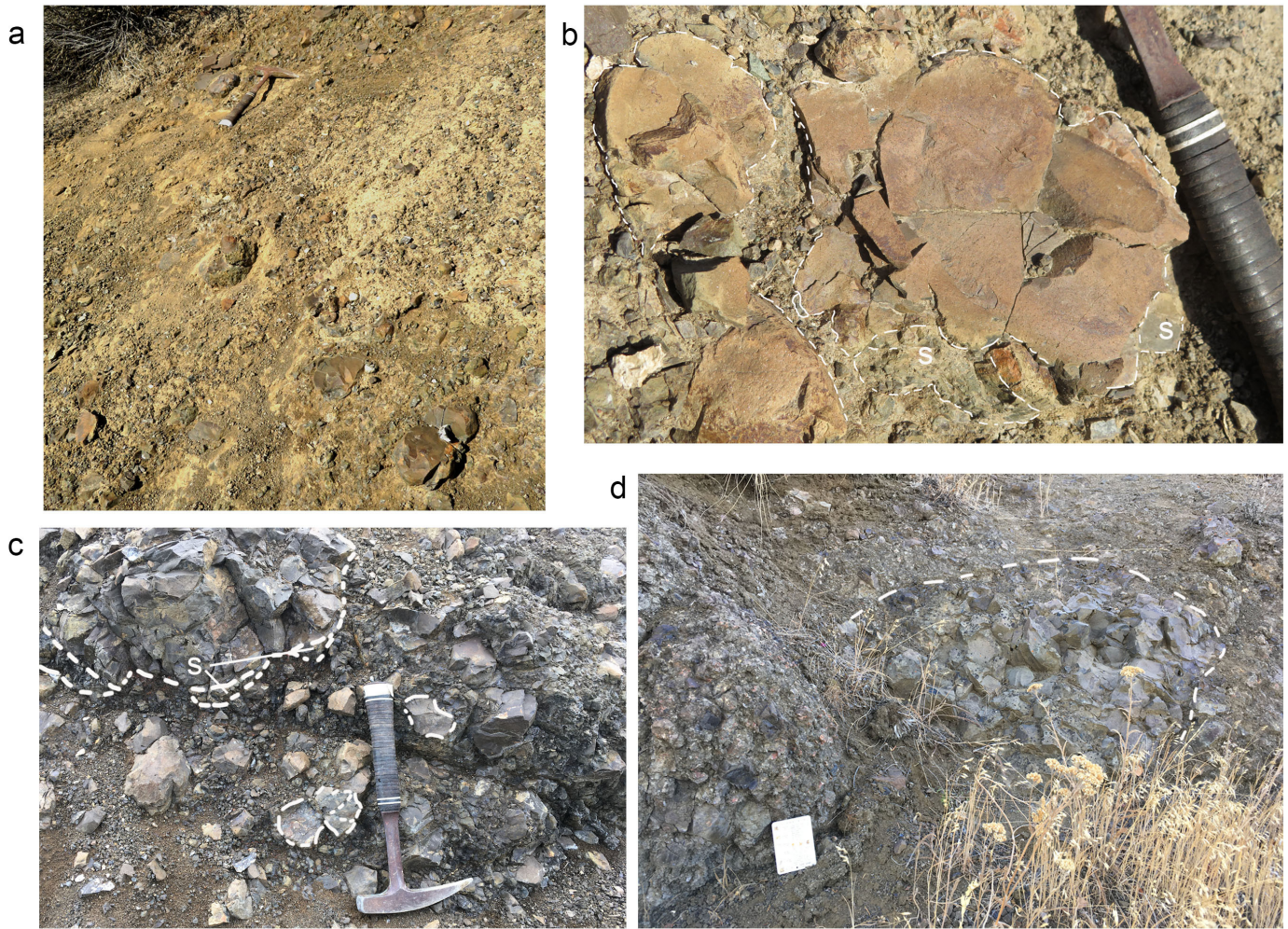


Fig. 5. Kenna Cartwright Park, andesitic breccias and pillow breccias of the Kissick Formation (Dewdrop Flats Formation). **a)** Lower part of Kissick Formation, monolithic pillow breccias comprising spherical and broken andesitic pillow fragments in a poorly sorted matrix of angular fine ash to block (10-15 cm) vitric and aphanitic fragments with curvilinear margins. Vague bedding (from upper right to lower left) is defined by alignment of larger and more intact pillow fragments. **b)** Lower part of Kissick Formation, a larger pillow broken into polyhedral blocks as a result of quench fragmentation and remobilized following fragmentation, as indicated by the separation along the cracks. A portion of the formerly glassy selvage (S) remains attached though most spalled off during fragmentation. **c)** Lower part of Kissick Formation, broken pillow in the upper left with partial selvage (S) in a hyaloclastite matrix, as described in a). The two smaller fragments are outlined to show the curvilinear margins and jigsaw fit of fragments. **d)** Upper part of Kissick Formation, andesitic flow lobe (outlined) internally broken into polyhedral blocks likely as a result of rapid cooling in contact with water, surrounded by a cogenetic monolithic breccia, similar to a) and c) but also containing a mix of both angular and bulbous forms, and non-vesicular to highly vesicular fragments; card is 9 cm long.

but internally fractured lava forming large pods up to 3-4 m long and 1-2 m thick. Surrounding monolithic breccias are similar to those elsewhere in the sequence but contain minor amounts of finer particles and are a mix of non-vesicular to highly vesicular fragments (Fig. 5d). Although glassy margins were not observed, the combination of deposit types resembles those formed along modern shorelines where aa flows enter a standing body of water (Yamagishi, 1991; Stevenson et al., 2012). These breccias may represent a combination of phreatic fragmentation, possibly from rootless cones, autobreccias, and hydroclastic fragmentation (e.g., Walker, 1992; Reynolds et al., 2015).

3.2. Cinnamon Ridge pillowed flows and hyaloclastite (Middle member, Tranquille Formation)

Pillowed flows are well exposed at Cinnamon Ridge north of the Thompson River in the Tranquille River canyon, and a canyon east of the Tranquille River (Fig. 2a). The flows form resistant mounds and hillside outcrops of closely packed pillows of various morphologies which grade laterally and vertically (in places) to abundant monolithic and altered hyaloclastite breccia. The hyaloclastites weather more easily and form gentler slopes.

The pillows are primarily aphyric and up to 2.5 m in diameter, with the large size possibly indicating high lava

fluxes (e.g., Hungerford et al., 2014). The pillows display two morphologies. In one variety, bulbous to spherical pillows become smaller upsection (Fig. 6a) and exhibit corrugated surfaces formed by expansion of the pillow after formation of the crust (Fig. 6b; see Yamagishi, 1987; Goto and McPhie, 2012), a feature that is more common in higher viscosity lavas, which cause the crust to break rather than expand with inflation (Walker, 1992). These pillows are solid, lacking central cavities, and exhibit a concentric structure defined by variations in colour and grain size (Fig. 6c). The spherical pillows are directly overlain by a thick (approximately 3 m) massive lava flow, lacking basal brecciation, suggesting either very high lava flux, or sudden draining of the lake in which the pillows formed. In the other variety, pillows are tubular and display more elliptical cross sections. These elliptical pillows exhibit radial fractures and are both filled and hollow with horizontal shelves reflecting significant inflation followed by drainage (Fig. 6d; see e.g., Hungerford et al., 2014). In both varieties, palagonitic former glassy pillow margins are well preserved, and there is little inter-pillow hyaloclastite (Figs. 6c, d).

The hyaloclastite comprises angular fine- to coarse-lapilli that were formerly glassy and now altered to palagonite, in a matrix of clays formed by alteration of the hyaloclastite. This type of hyaloclastite is formed by quench fragmentation of effusively erupting lava encountering water (e.g., Yamagishi, 1987). The field relationships indicate that the hyaloclastites are spatially and temporally related to the pillows and likely formed about the same time due to quench fragmentation of pillowed flows.

3.3. The Nipple

3.3.1. Nipple breccia, Dewdrop Flats Formation

At the type locality, north of the east side of Kamloops Lake (Fig. 2), the Nipple volcanic breccias (Fig. 7; Ewing, 1981a), are exposed in a belt 0.25-1.5 km wide, and 3.5 km long, trending roughly N10°E with a cone-shaped edifice about 300 m in diameter near the northern extent of the exposure (the Nipple). These breccias are the most mineralogically and texturally distinct rocks in the area. In general, they are olivine and pyroxene phyric (3-15%, mostly 2-3 mm, but up to 1 cm) with plagioclase microlites (1-3%, increasing upsection), vesicular to scoriaceous, basaltic-andesite lapilli tuff to tuff breccia (Fig. 7a).

The thickest exposure of the Nipple is at the cone where the breccia is about 275 m thick. Exposures north and south of the cone are about 130 to 180 m thick. At the cone, the breccia consists primarily (98%) of lapilli- to bomb-sized clasts (75-80%) that are blocky to rounded (breadcrust to cannonball morphologies; see e.g., Alvarado et al., 2011). The breccia is clast supported with finer coarse-ash and smaller lapilli-sized particles filling spaces between the cm-scale bombs. Matrix clays are the result of in-situ alteration of smaller fragments rather than depositional (Fig. 7a). Some of the clasts exhibit internal fracturing, possibly due to impact. Rare cognate clasts are angular (Fig. 7b), but otherwise similar to the juvenile

clasts. Near the top of the exposure are larger bombs and bomb slabs, some draping the underlying breccia (Fig. 7c), and this inverse grading might signify a decrease in the explosivity as the cone evolved (e.g., Alvarado et al., 2011). Away from the cone, the pyroclastic breccias undergo a facies change to a flow breccia comprising a mix of large round, or pillow-shaped clasts up to about 10-30 cm that are internally brecciated with curvilinear fractures, and smaller blocky fragments down to coarse-ash in size (Fig. 7d) where it overlies thinly bedded and laminated tuffaceous sediments that were described by Ewing (1981a) as aquagene tuffs.

3.3.2. Kissick breccias, Dewdrop Flats Formation

The Kissick breccia overlies the Nipple breccia about 2 km south of the cone where it is best exposed as part of a resistant ridge (Figs. 2, 8). The breccia is heterolithic comprising about 3-5% small, 1-4 cm angular accidental fragments of carbonate-cemented siltstone, and 95% andesitic juvenile and cognate pyroclastic fragments. The juvenile and cognate fragments, though compositionally monolithic, display a variety of morphologies ranging from ameboid (Fig. 8c) to more angular broken bomb-shaped fragments, some of which have scoriaceous cores. The matrix is poorly sorted (lapilli to coarse-ash-size) and comprises angular, non-vesicular fragments with curvilinear margins (Figs. 8d-e). In places nearby fragments show a jig-saw fit, and some display 1-3 mm thick reaction rims. The unit is very vaguely bedded, with bedding defined by the long axes of some of the larger fragments (Fig. 8d). In contrast to the Kissick member observed at Kenna Cartwright Park (Figs. 2a, 5), the breccias here are interpreted to represent emplacement of an andesitic dome or sub-volcanic intrusion. These features may record interactions of rising magma with water, causing varying degrees of magmatic and phreatomagmatic to hydroclastic and autoclastic fragmentation (see e.g., Smellie et al., 1998).

3.4. Doherty Creek and Castle Butte, Dewdrop Flats Formation

The Doherty Creek member is exposed northwest of Kamloops Group type area, where it is in gradational contact with the Castle Butte member along its southern margin (Figs. 2, 3). From a distance the flows appear to form relatively continuous layers with gentle depositional dips (Fig. 9a). In detail, the flows are highly brecciated, discontinuous along strike, and intruded by northeast-trending dikes that dip steeply to the north and form distinct ridges (Fig. 9b). Near the contact with the Castle Butte member, a coherent Doherty Creek member flow about 3 m thick (Fig. 9c) changes vertically and laterally from an autobreccia to hyaloclastite breccia. The flow is aphyric, and sparsely vesicular with 1-3 mm diameter spherical vesicles comprising 5% of the flow, along with larger gas cavities 0.5 to 1 m in diameter that are filled and lined with quartz. Above this flow are several metres of coarse breccia which may be an autobreccia, similar to the Red Plateau member (section 3.5.; Figs. 9d, e). This breccia of the Doherty Creek member fines

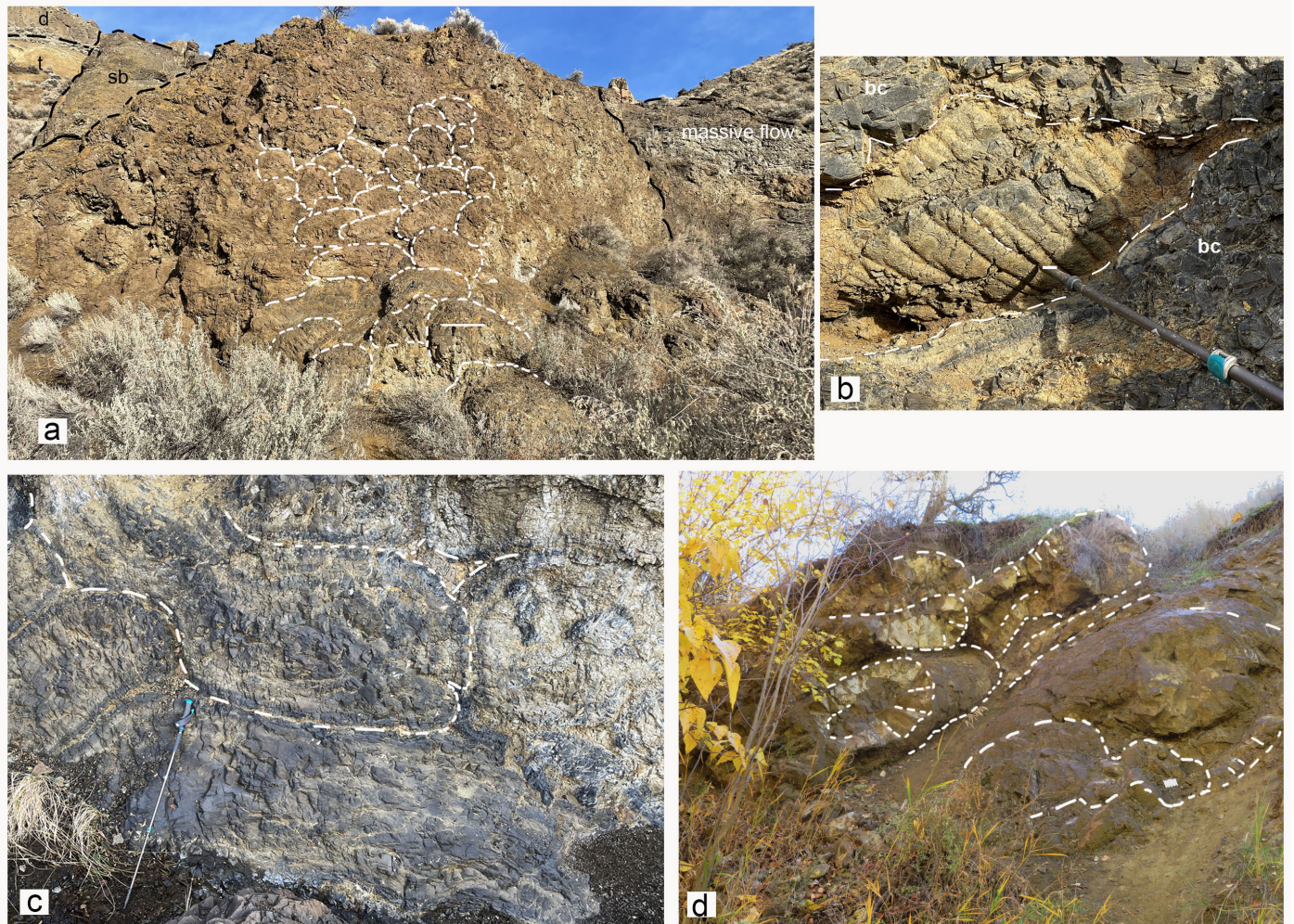


Fig. 6. Cinnamon Ridge pillowed flows showing two different morphologies. **a)** Bulbous, closely packed pillows showing an overall decrease in size upward. Behind the pillows is a slump block (sb) of tube-fed pillows, tuff (t), and a dike (d). The scale bar is 1 m. **b)** Corrugated surface of a pillow likely formed by expansion of the interior of the pillow after formation of the initial crust. The smooth broken crust (bc) is on both sides of the corrugated surface. The bar scale at the tip of the walking stick is 1 cm. **c)** Concentrically zoned pillows with more elongate shapes, and minimal inter-pillow breccia. The walking stick is 1.1 m. **d)** Tubular pillows showing radial cracks, and one hollow tube (back right). The card at the bottom of the photo is 9 cm long.

along strike to the east where it was previously mapped as the Castle Butte member (Ewing, 1982). Within the Castle Butte member lakebed shales form an isolated pod about 10 by 5 m that is overlain by a felsic tuff forming a discontinuous bed 5 m thick, which in turn is overlain by fine hyaloclastite.

3.5. Red Plateau member, Dewdrop Flats Formation

The Red Plateau member was mapped as an upper unit of the Dewdrop Flats Formation (Fig. 3; Ewing, 1981a). Where observed at two sites near the Red Plateau (Fig. 2), this unit forms a series of andesitic flows more than 2.5 m thick. These flows are dark grey and primarily plagioclase phyric with plagioclase crystals up to 1 cm. The flows have massive, sparsely vesicular interiors, some being highly crystalline, and brecciated flow tops about 1-2 m thick (Fig. 10a). The flow top breccias comprise angular to subangular scoriaceous fragments 1-30 cm with no matrix (Figs. 10b, c). There are

sparsely disseminated sulphides in one of the flows at Wheeler Peak. The Red Plateau member covers an aerial extent of about 50 km², which is about 25% of the type area of the Kamloops Group (Ewing, 1981a, 1982).

3.6. Opax breccia member, Dewdrop Flats Formation

The Opax breccia is the uppermost member of the Dewdrop Flats Formation (Fig. 3; Ewing, 1981a). It is exposed in five separate localities on hilltops, forming a roughly east-west trend, where it overlies the Red Plateau member at all except the northwest corner of the type area where it overlies the Doherty Creek member (Ewing, 1981a, 1982). The Opax breccia at Wheeler Peak (Fig. 2), is monolithic, poorly sorted, and clast supported with little matrix. Fragments are andesitic, grey, vitric to aphanitic, angular, mm to a few cm in size and internally brecciated. Some of the vitric fragments exhibit flow banding. The apparent matrix is caused by alteration,

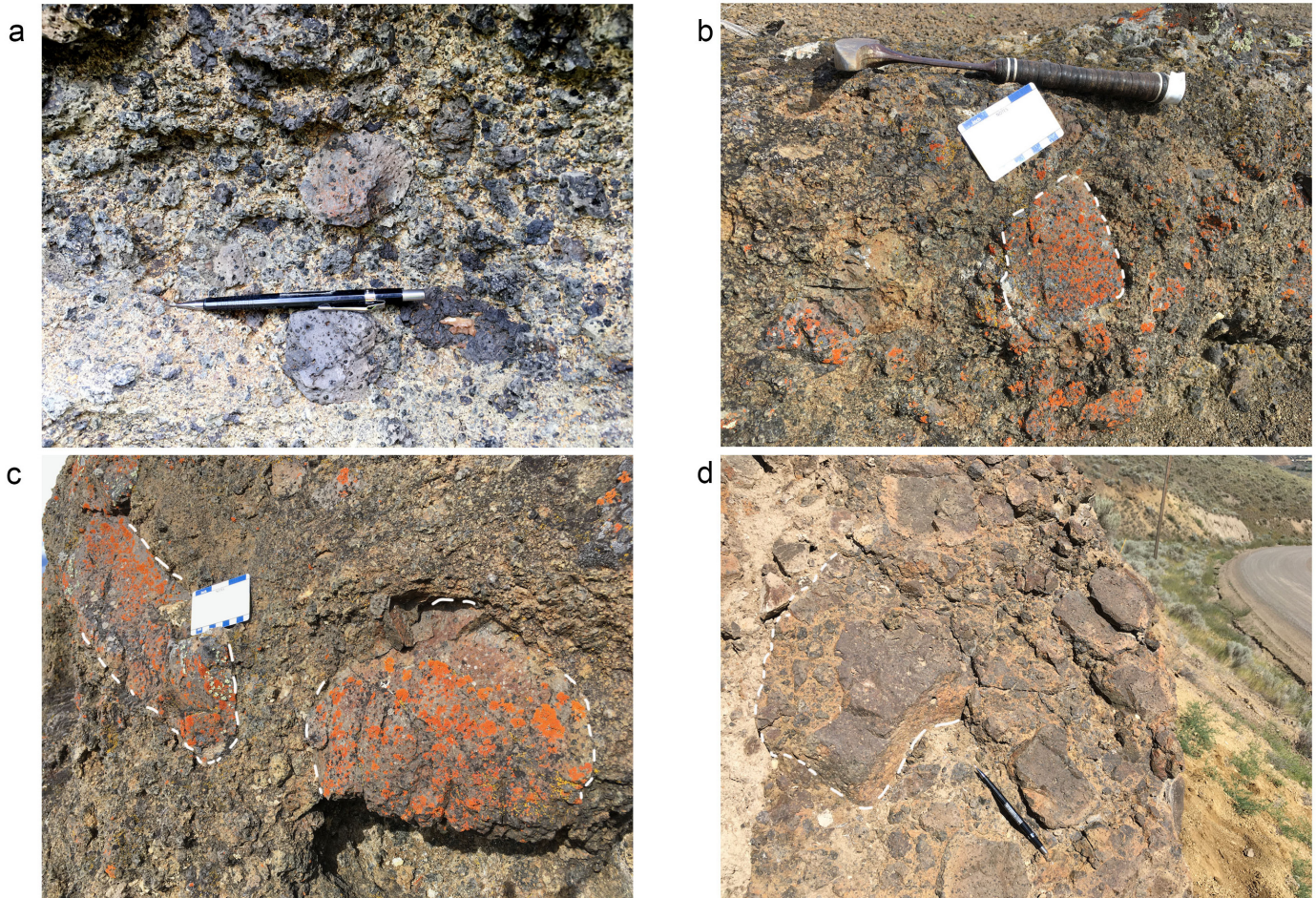


Fig. 7. The Nipple breccia (Dewdrop Flats Formation). **a)** Pyroclastic fragments near the base of the pyroclastic cone showing the spherical shape of some ejecta, and the variation in size of ejecta. The clay matrix is not depositional, but the result of in-situ alteration of finer vitric fragments (i.e., pseudomatrix). **b)** Angular cognate clast in the mid-portion of the Nipple breccia. **c)** Large slabs and bombs at the top of the cone. **d)** Hyaloclastite flow breccia showing one large fragment that is internally brecciated.

and alteration rims 1-2 mm thick are evident on some of the fragments (Fig. 10d). Though the area is largely barren of mineralization, finely disseminated sulphides occur in some of these rocks. Based on major element geochemistry (Ewing, 1981a, c), the Opax breccia is a trachyandesite, making it the most silicic unit in the Kamloops Group type area.

4. Geochemistry

Samples for whole rock geochemistry were collected from multiple Kamloops Group exposures between 2017 and 2019 (Fig. 2). Below we summarize the results from only two sites, Kenna Cartwright Park (two flow samples from the Border facies at the base of the Kamloops Group; six samples from the Mara Hill member of the Dewdrop Flats Formation) and Cinnamon Ridge (two pillowed flows from the middle unit of the Tranquille Formation; Fig. 2). We avoided collecting from more heterolithic pyroclastic units to better enable petrogenetic interpretations. A full description of the analytical methods and the complete dataset will be presented elsewhere (Van Wagoner and Ootes, 2021).

4.1. Methods

Clean, alteration-free samples were submitted to Actlabs in Ancaster, Ontario, for bulk-rock major, trace, and rare earth element analysis. At Actlabs, samples were crushed to pass 2 mm, mechanically split using a rifle splitter, and pulverized using mild steel to 95% passing 105 μm (Code RX-2). Major element oxides were determined using inductively coupled plasma optical emission spectroscopy (ICP-OES) and trace element concentrations were determined using fusion inductively coupled plasma mass spectrometry (ICP-MS; Code 4 Lithoresearch). Measurement accuracy was determined using certified standards provided by Actlabs and blind samples of the British Columbia Geological Survey till standard.

4.2. Results

Based on the total alkali-silica (TAS) diagram (re-calculated to 100% volatile-free basis), the Kamloops Group rocks are classified as andesite to dacite (Fig. 11a). The samples have 2.37 to 8.41% loss on ignition and because of the high volatile content this study relies mostly on the immobile trace elements



Fig. 8. The Kissick breccia (Dewdrop Flats Formation) where it overlies the Nipple breccia. **a)** At the ridge top, a typical exposure of possible sub-volcanic intrusions in the type area; in foreground are Quaternary drift deposits exposed in a road cut. **b)** Close up of a) showing sub-horizontal joints. **c)** Ameboid-shaped volcanic fragment with internal polyhedral joints. The smaller fragments in the matrix are the same composition and shape as the fragments comprising the larger form. The dark fragment near the point of the hammer is relict glass. **d)** Two tabular fragments on the right side of the photo are aligned parallel to vague bedding. The lower fragment is lighter coloured aphyric, aphanitic andesite, the upper is relict glass; both are internally brecciated. The outlined fragment displays a cusped-lobate outline, preserves a vitric margin, exhibits flow banding, and is internally fractured. **e)** Broken bomb with scoriaceous interior surrounded by breccia.



Fig. 9. The Doherty Creek member (Dewdrop Flats Formation) near Doherty Creek. **a)** General exposure of the Doherty Creek member. **b)** Flow breccia (fb) cut by vertical dike with near-horizontal columnar joints. **c)** Core of an aa flow surrounded by autobreccia. **d)** Close up of autobreccia showing a combination of angular and more spherical fragments and a combination of highly vesicular fragments (mostly intensely weathered) and dense non-vesicular fragments. Clay material between fragments formed by weathering of finer particles and is not depositional matrix. **e)** Breccia that has features resembling hyaloclastite, particularly fragments with curvilinear margins and internal fractures.

to classify the rocks (e.g., MacLean and Barrett, 1993). All of the rocks plot in the calc-alkaline field in a tholeiitic versus calc-alkaline discrimination diagram (Fig. 11b). They range from basalt to basaltic-andesite and trachy-andesite and are subalkaline to weakly alkaline; four of the flows from the Lava flow field are the most alkaline (Fig. 11c).

The rocks span a range of SiO_2 from 59 to 66 wt.% (recalculated to 100%, LOI free; Figs. 11, 12). In general, there is an increase of SiO_2 with $\text{Na}_2\text{O}+\text{K}_2\text{O}$ (Fig. 11a), but little relationship between SiO_2 and Al_2O_3 (Fig. 12a). There is an inverse relationship between MgO and SiO_2 , and a slight decrease in FeO(T) , and TiO_2 , which is less clear. However, there is a distinct positive increase of $\text{CaO}/\text{Al}_2\text{O}_3$ with increasing CaO (Fig. 12f). Similarly, immobile compatible elements Co, Cr, V, Ni, and Sc decrease with increasing Zr/TiO_2 , used here as an indication of fractionation (Fig. 13), but the relationship with Sr is less clear. Relative to chondrite, the rocks are light-

REE (LREE) enriched ($\text{La}/\text{Yb}_N=13-22$) with a relatively flat heavy-REE (HREE) pattern ($\text{Dy}/\text{Lu}_N=1.4-1.7$) and no Eu anomalies (Fig. 14a). Relative to primitive mantle, all of the rocks are enriched in large ion lithophile elements (LILE), with prominent positive Ba, K, and Pb anomalies, and to a lesser extent U and Sr, and with enrichment of the LREE with respect to the HREE. High field strength elements (HFSE) Nb and Ta display negative anomalies, without distinct negative Zr or Ti anomalies (Fig. 14b).

Strontium values are relatively high, from 453-1144 ppm (Fig. 13f) and Ba ranges from 1205 to 2022 ppm, with the highest values being from the two pillowed flows. The samples are enriched in the fluid mobile LILE, compared with the less fluid mobile HFSE and REE (e.g., Ba/La; section 5.3.). Conversely, these samples have low immobile to mobile element ratios (e.g., Ce/Pb [9-11]), and immobile incompatible element ratios (e.g., Th/Yb, Nb/La; section 5.3.). Most of the

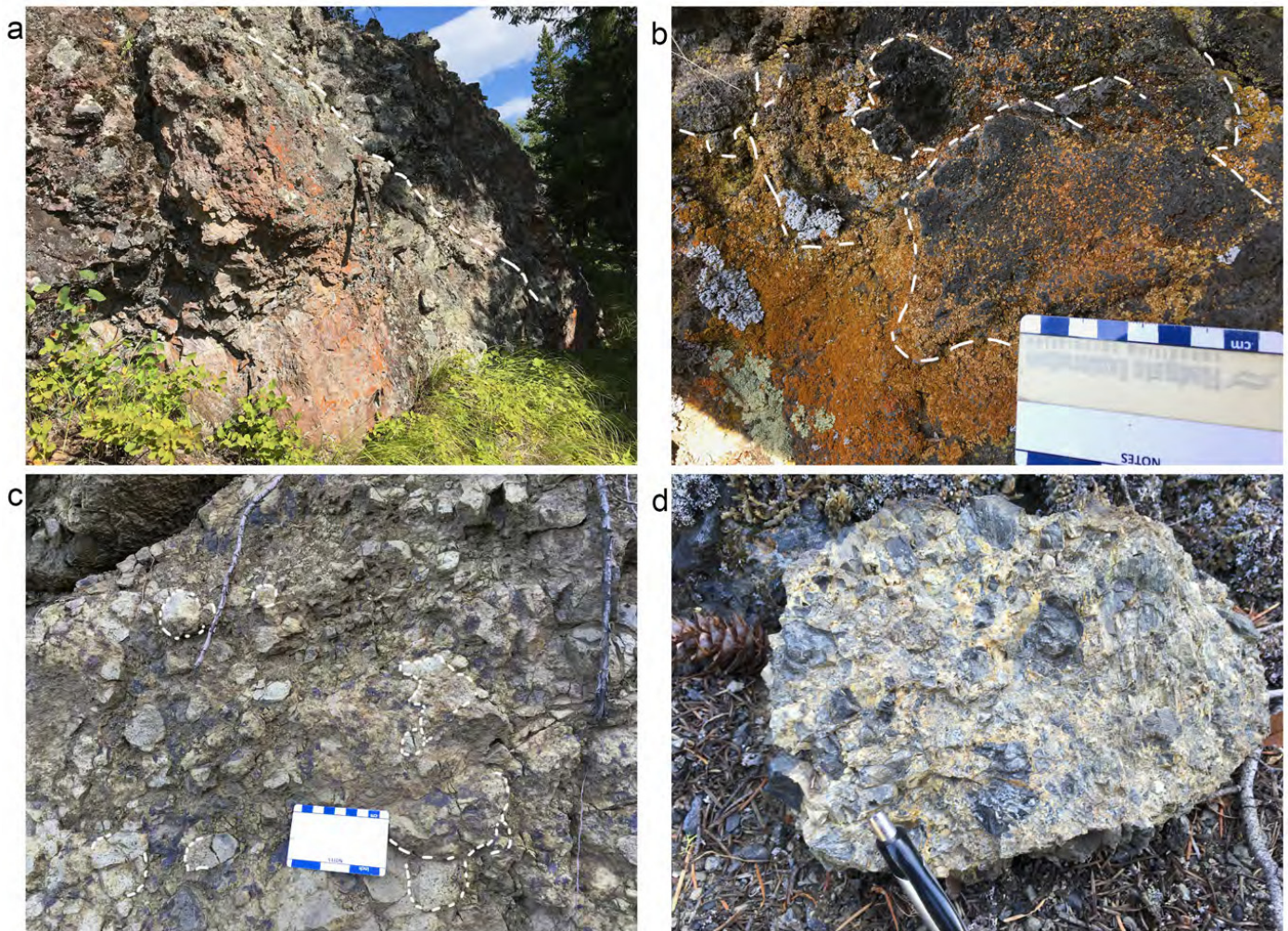


Fig. 10. Red Plateau member (a-c) and Opax breccia member d) (Dewdrop Flats Formation. **a**) Thick flow showing the contact (dashed white line) between the more massive part of the flow and overlying autobreccia. **b**) Highly scoriaceous flow top breccia with lichen exploiting vesicles. Fragments are angular to subspherical there is no matrix. **c**) Autobreccia that is less scoriaceous than b), with a mix of clast sizes and vesicularity. Some of the fragments are outlined to show a combination of spherical fragments lacking internal brecciation and more angular fragments that also display internal fragmentation. **d**) Opax breccia showing flow banding in some fragments and an altered matrix.

rocks have adakite-like compositions in terms of relatively high SiO_2 , Al_2O_3 , Na_2O , and MgO (Figs. 11a, 12). All have $\text{Sr} > 400$ (Fig. 13), and all but one sample has $\text{Sr}/\text{Y} > 40$, $\text{Yb} < 1.9$, and $\text{La}/\text{Yb} > 20$. Absolute values of Y are up to 22 ppm, slightly higher than typical adakites (Zhang et al., 2019).

5. Discussion

5.1. Physical volcanology

The Kamloops Group volcanic rocks include a combination of effusive and explosive volcanic rocks that preserve evidence for magma-water interaction. This includes phreatic and phreatomagmatic textures and a variety of in-situ hyaloclastites. Some of the volcanic horizons are associated with lakebed sediments and water-lain tuffs, but little evidence of peperitic breccias was observed during sampling. The sedimentary rocks and pillow basalts provide evidence of sub-aqueous volcanism, but specific relationships of the lakes to volcanic

activity remains unknown. For example, did the lakes originate solely in graben topographic lows or might some be related to lava flow dams or caldera? Forthcoming facies mapping and volcanological studies will clarify volcanic processes and the three-dimensional evolution of volcanism of the Kamloops Group, along with its extent and relationship to coeval volcanism of south-central British Columbia.

5.2. Fractionation trends

The variation diagrams can be used as an indication of the relative importance of fractionating phases. The positive relationship of increasing $\text{CaO}/\text{Al}_2\text{O}_3$ to CaO (Fig. 12f) is indicative of pyroxene fractionation. The decrease of Co, Cr, and Ni with Zr/TiO_2 (Fig. 13) reflects olivine and pyroxene fractionation. There is a slight decrease of FeO(T) with increasing SiO_2 (Fig. 12c) and Ti with Zr (not shown) suggesting some fractionation of Fe-Ti oxides. The decrease

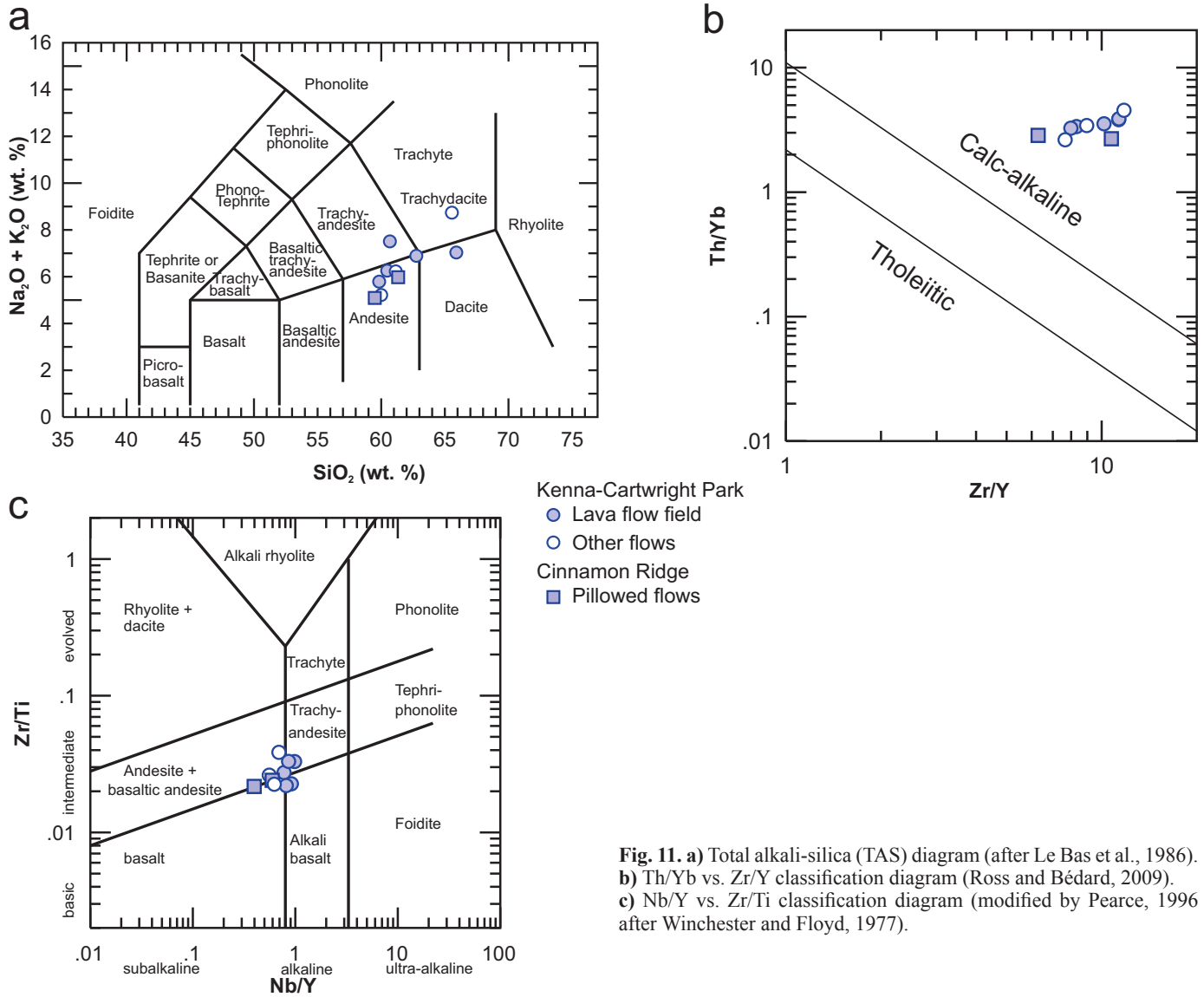


Fig. 11. a) Total alkali-silica (TAS) diagram (after Le Bas et al., 1986). b) Th/Yb vs. Zr/Y classification diagram (Ross and Bédard, 2009). c) Nb/Y vs. Zr/Ti classification diagram (modified by Pearce, 1996 after Winchester and Floyd, 1977).

of V with increasing Zr/TiO₂ (Fig. 13c) is prominent and may be partially controlled by Fe-Ti oxide fractionation. However, V also partitions into clinopyroxene and amphibole, although partition coefficients of V are influenced by oxygen fugacity, volatile phases, and temperature (Laubier et al., 2014; Wang et al., 2019; Iverson et al., 2018), as does Sc (Vander Auwera et al., 2019). The strong decrease of both Sc and V with Zr/TiO₂ (Fig. 13), suggests that pyroxene and probably amphibole fractionation influenced their concentrations. The lack of a strong co-variation of Al₂O₃ with SiO₂ (Fig. 11a) and lack of negative chondrite-normalized Eu anomalies (Fig. 14a) indicates that plagioclase was not an important fractionating phase compared with olivine and pyroxene. The absence of a relationship between P₂O₅ and SiO₂ (Fig. 12e) indicates that apatite fractionation was insignificant.

5.3. Geochemical comparison of the Kamloops, Princeton, and Pentiction groups

Eocene volcanic rocks in southern British Columbia are separated into the Kamloops, Princeton, and Pentiction groups (Fig. 15). However, the basis for this separation and the stratigraphic relationships between these units remains unclear. Geochemistry, paired with stratigraphic mapping, and high-precision geochronology has the potential to address this problem. Although data are sparse, particularly from the Pentiction Group (Fig. 15), some first-order comparisons can be made.

Rocks of the Pentiction Group are potassic, alkaline basaltic trachyandesites to tephriphonolites (Dostal et al., 2003). The Kamloops and Princeton groups are mostly calc-alkaline to moderately alkaline (Figs. 11b, c; Breitsprecher, 2002; Ickert et

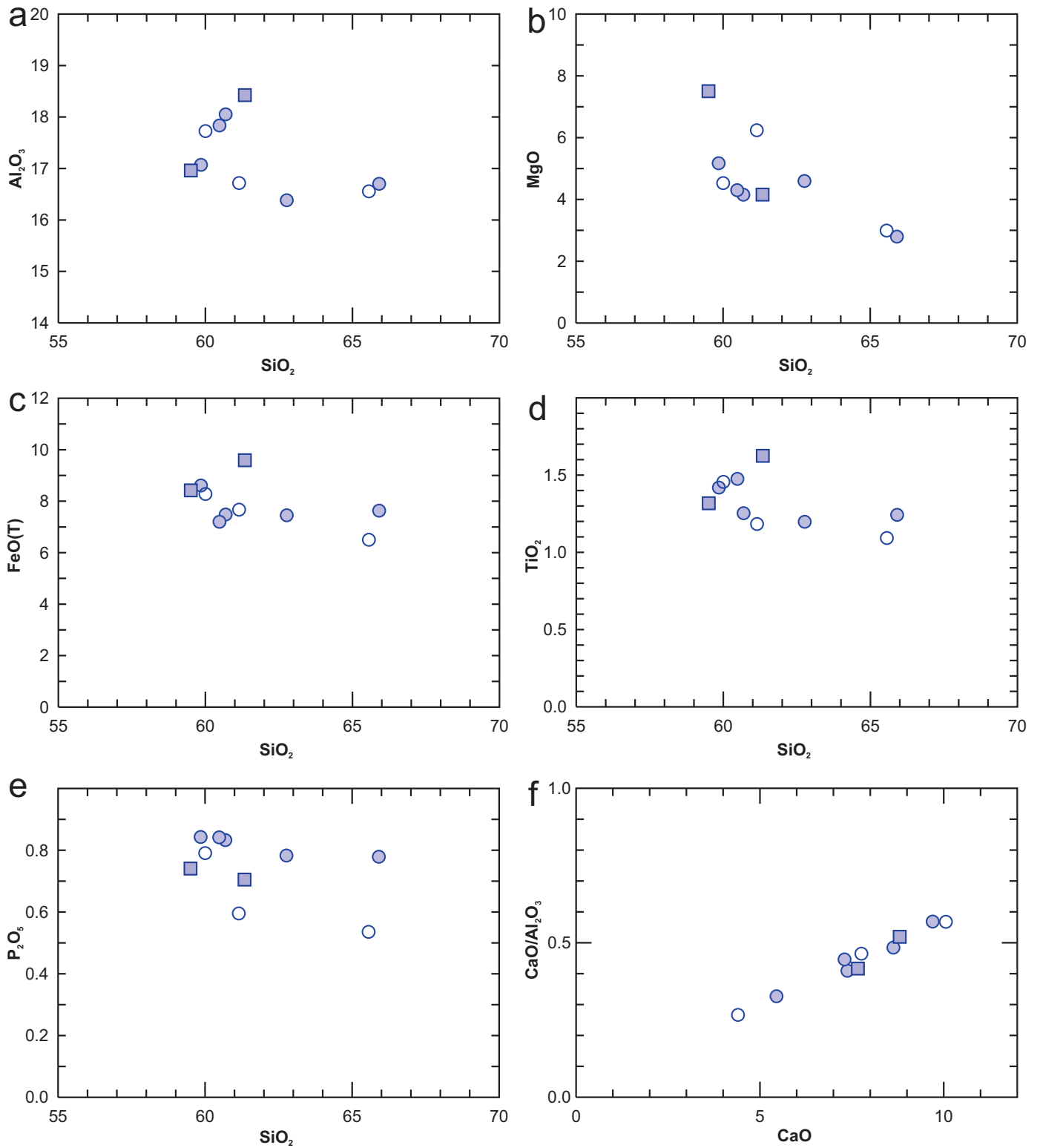


Fig. 12. Harker diagrams. Major elements (wt.%) are corrected to 100% volatile free. SiO₂ vs. **a)** Al₂O₃, **b)** MgO, **c)** FeO(T), **d)** TiO₂, **e)** P₂O₅, and **f)** CaO vs. CaO/Al₂O₃.

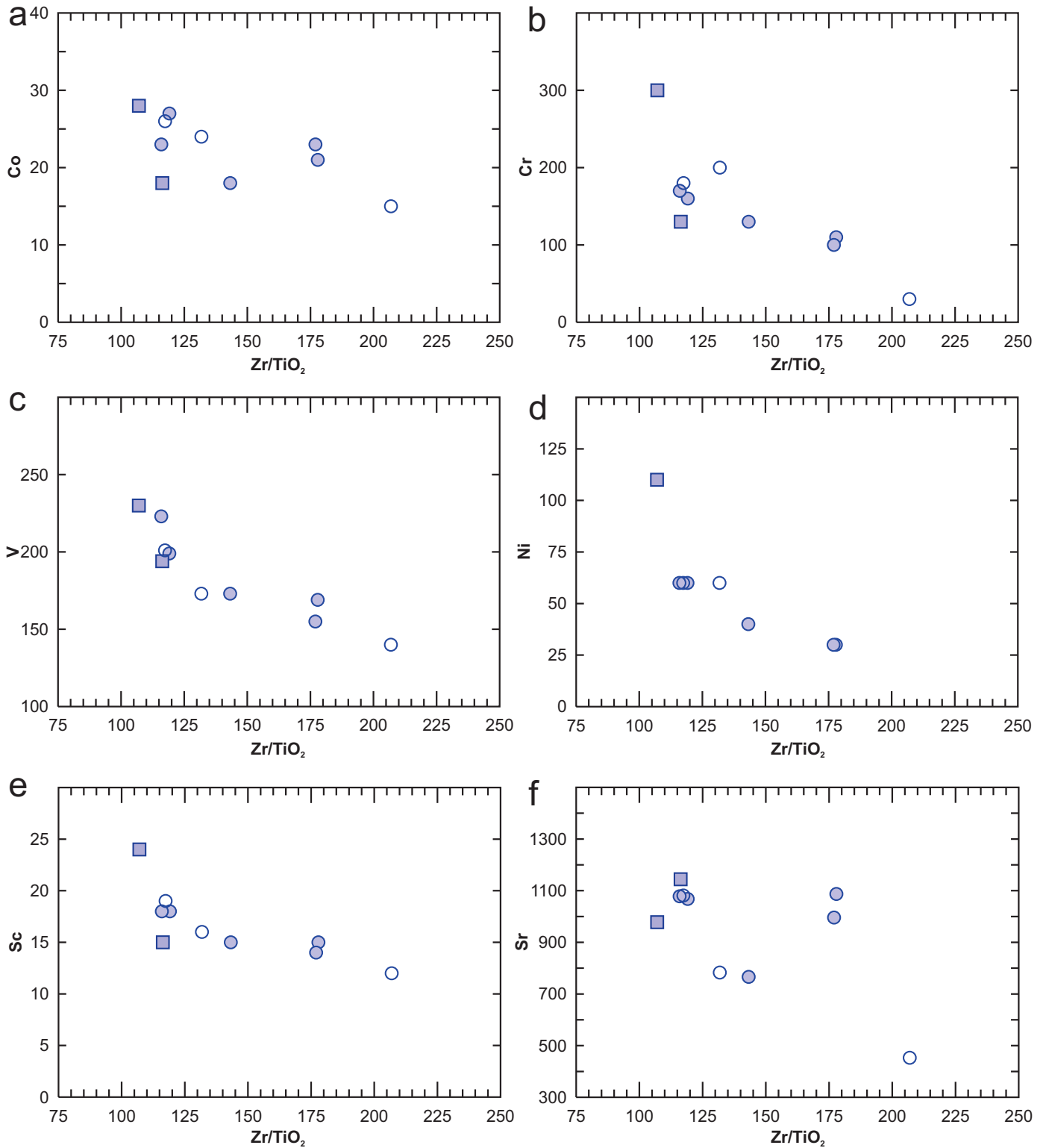


Fig. 13. Trace element variation diagrams. Zr/TiO₂ vs. a) Co, b) Cr, c) V, d) Ni, e) Sc, and f) Sr.

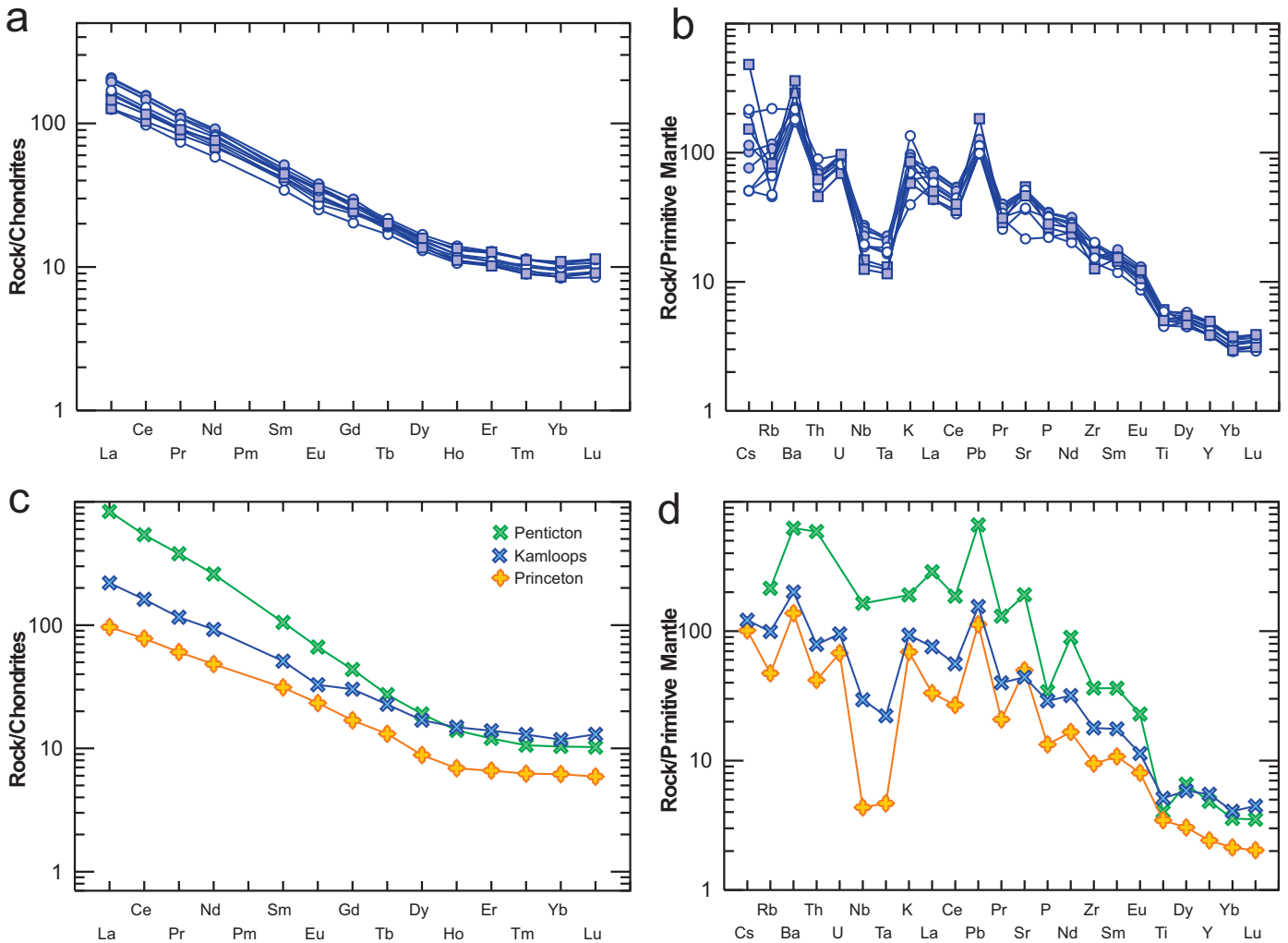


Fig. 14. **a)** Chondrite-normalized REE. **b)** Primitive mantle-normalized trace and REE for samples from this study. **c)** Chondrite-normalized REE and **d)** Primitive mantle-normalized trace and REE for median values (<63 wt.% SiO₂) for rocks of the Kamloops, Pentiction, and Princeton Groups. Data from this study, Breitsprecher (2002), Dostal et al. (2003, 2019), and Ickert et al. (2009). Normalizing values are from Sun and McDonough (1989).

al., 2009), and both have adakitic characteristics. Rocks from all three units are LREE enriched, with flat HREE chondrite-normalized patterns, and have similar primitive mantle-normalized trace element characteristics, with the major difference being the negative anomalies of Nb and Ta that are lowest in the Princeton Group and minimal in the Pentiction Group (Fig. 14).

Trace element ratios can give an indication of the mantle source and depth of melting. Almost all the rocks from all three groups have flat HREE patterns and steep LREE patterns with some variations (Figs. 14, 16a). The REE patterns for the Kamloops Group are fairly uniform and the Princeton Group parallel, but with lower total REE and less enrichment of the LREE (Figs. 14, 16-18). The Pentiction Group has higher LREE enrichment, related to smaller degrees of partial melting (Figs. 14, 16-18). The overall LREE-enriched and flat to slightly elevated HREE patterns indicates variable amounts of garnet in the source (Fig. 16a; see Wang et al, 2002; Davidson

et al., 2007; Keskin et al., 2012; Maro and Caffè, 2016; Dostal et al., 2019).

Melts that form in equilibrium with amphibole have lower Rb/Sr and higher Ba/Rb than those that form in equilibrium with a phlogopite-bearing source (Fig. 16b; e.g., Furman and Graham, 1999; Liang et al., 2017). All of the rocks display ratios that are consistent with an amphibole-bearing source (Fig. 16b). The probable source for the Kamloops Group was amphibole-bearing lherzolite near the garnet-spinel transition, at depths of 70-90 km (Dostal et al., 2019), with consistent degrees of partial melting (Figs. 16a-c). The low Nb and other HFSE, which are depleted in the lithospheric mantle with respect to LREE, do not support an asthenospheric mantle source for the three groups (Fig. 16c; Bradshaw and Smith, 1994; Smith et al., 1999; Aydinçakir and Sen, 2013). Similarly, there is no evidence that they fall on a MORB-OIB array (Fig. 16d). The geochemical data support an origin in the subcontinental lithospheric mantle.

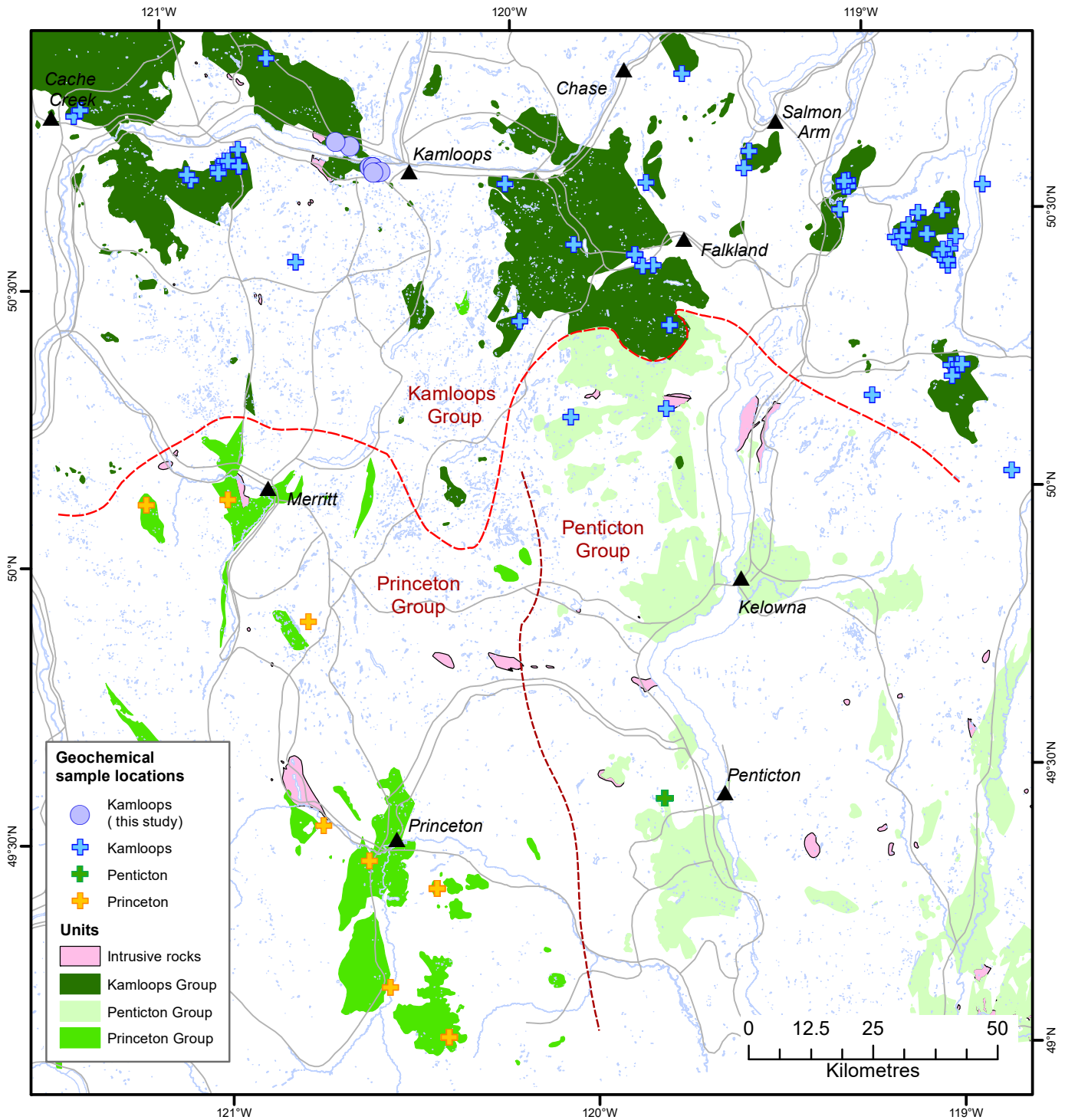


Fig. 15. Distribution of Eocene volcanic and intrusive rocks in south-central British Columbia. Sample locations for the Kamloops Group are from this study, Breitsprecher (2002), and Dostal et al. (2019). Princeton Group samples are from Ickert et al. (2009) and Penticton Group samples are from Dostal et al. (2003). The boundaries between the groups are shown with dashed red lines.

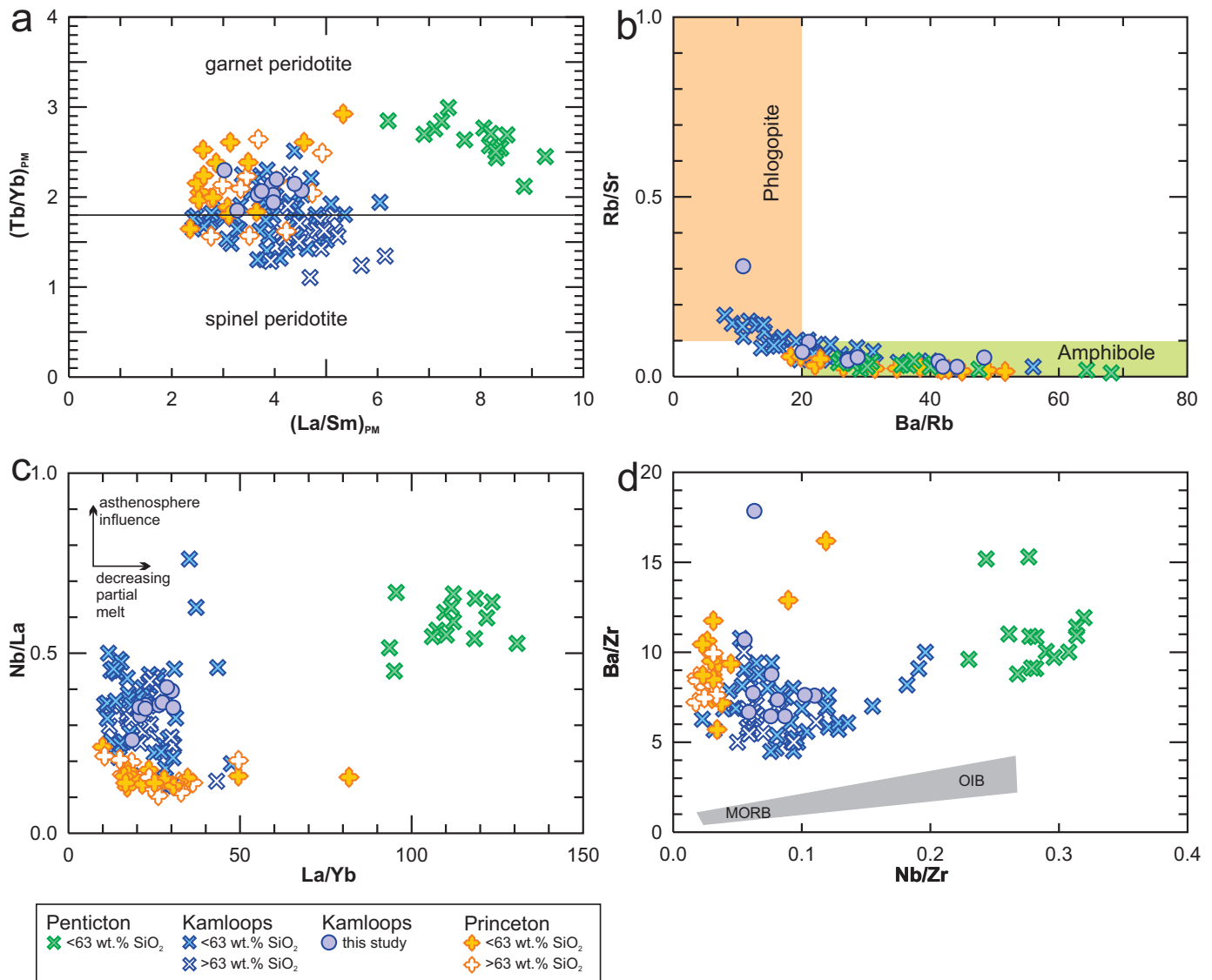


Fig. 16. a) Primitive mantle normalized $(La/Sm)_{PM}$ vs. $(Tb/Yb)_{PM}$. Relative depth of melting increasing with increasing $(Tb/Yb)_{PM}$. Modified from Wang et al. (2002) and Dostal et al. (2019). Normalizing values from Sun and McDonough (1989). **b)** Ba/Rb vs. Rb/Sr . Phlogopite and amphibole melting fields are from Furman and Graham (1999). Only rocks with <63 wt.% SiO_2 are plotted. **c)** La/Yb vs. Nb/La . Asthenosphere is characterized by $Nb/La \sim 1.2$ (after Smith et al., 1999). **d)** Nb/Zr vs. Ba/Zr . The MORB-OIB array is from Leeman et al. (2005). Kamloops data are from Breitsprecher (2002), Dostal et al. (2019) and this study; Princeton data are from Ickert et al. (2009); Pentiction data are from Dostal et al. (2003).

The primitive mantle-normalized trace element patterns (Fig. 14d) are typical of subduction-related rocks (Dostal et al., 2003; Ickert et al., 2009). The Kamloops and Princeton groups have low Nb/La and variable Th/Nb (Fig. 17a) indicating that fluids had a role in the melt source. The Pentiction Group has high Nb/La and uniform Th/Nb (Fig. 17a) indicating less of a role by hydrous fluids in the melt source. The variable Ba/La and low Th/Nb of the Kamloops and Princeton groups further indicate a role for slab-derived fluids in the melt source, whereas the Pentiction Group is more strongly influenced by sediment contamination or sediment in the melt source (Fig. 17b; see e.g., Walker et al., 2000, 2001; Woodhead et al.,

2001). The Pentiction Group Ba/La is still relatively high and indicative of an arc affiliation (e.g., Michelfelder et al., 2013). Similarly, the Princeton and Kamloops groups trend toward Ba/Th enrichment, whereas the Pentiction Group rocks have consistently low values (Fig. 17c). The U/Nb is not affected by crystal fractionation, such that significant increases in this ratio with SiO_2 can be used as an indication of crustal contamination (Fig. 17d; e.g., Krienitz et al., 2006; Dostal et al., 2019). Crustal contamination is more evident in the Princeton Group than in the Kamloops Group, but does not appear to have been significant for either unit (Fig. 17d). Overall, the Pentiction Group rocks have trace element signatures that are more

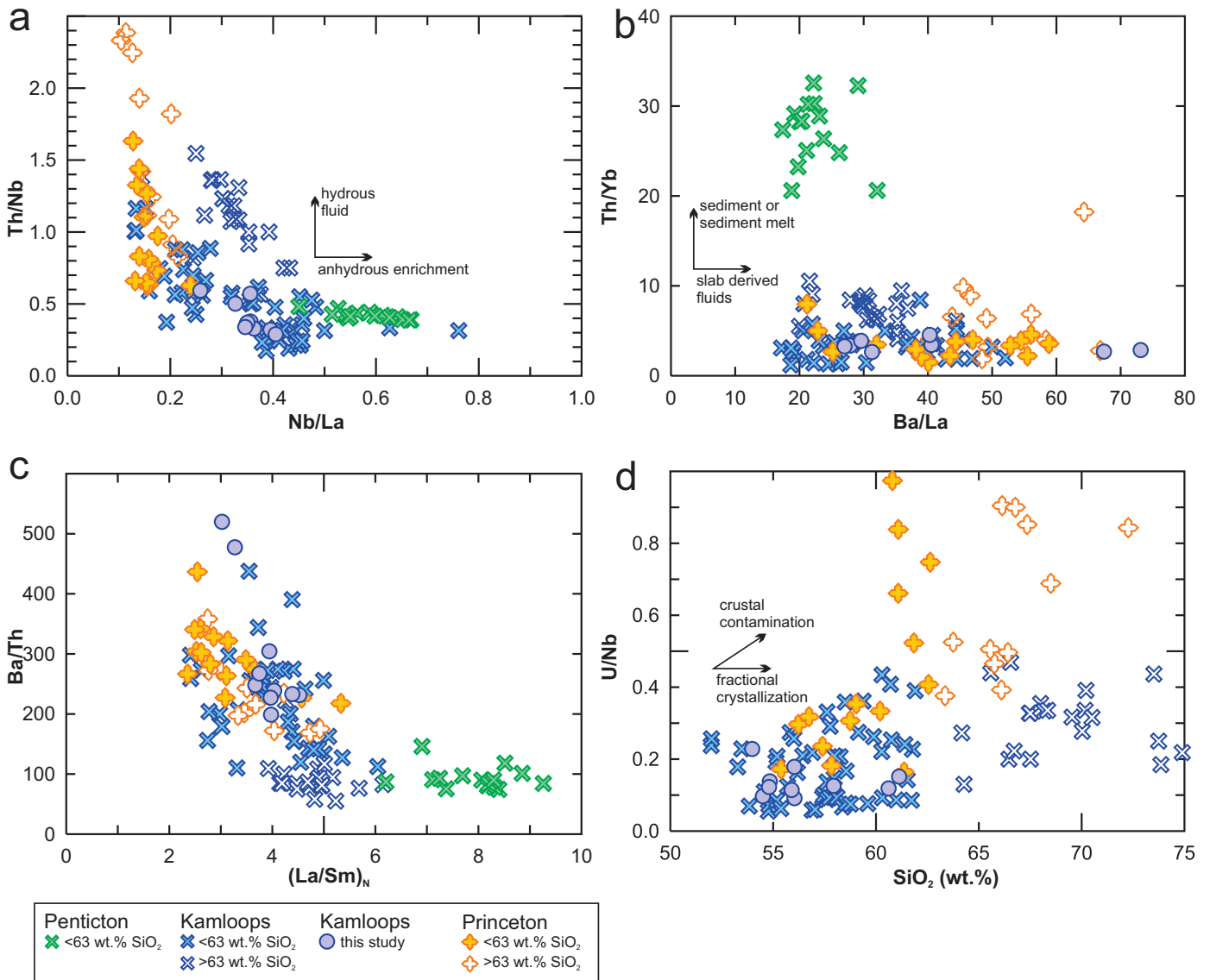


Fig. 17. Trace element and REE ratio diagrams. **a)** Nb/La vs. Th/Nb (Wang et al., 2016; Zhang et al., 2020). **b)** Th/Yb vs. Ba/La (Woodhead et al., 2001). **c)** Chondrite-normalized La/Sm vs. Ba/Th showing a decrease in Ba/Th with decreasing partial melting for all but the Pentiction Group. Chondrite normalizing values are from Sun and McDonough (1989). **d)** SiO₂ (wt.%) vs. U/Nb (Dostal et al., 2019); no U data are available for the Pentiction Group. Data sources as in Figure 16.

indicative of a mantle source influenced by anhydrous, melt induced metasomatism, whereas the Kamloops and Princeton groups reflect melting of a hydrous mantle source enriched by slab-derived fluids (Figs. 17 a-c).

Dostal et al. (2003) argued against crustal contamination as the cause of the trace and REE characteristics of the Pentiction Group and interpreted their evolved Nd and Sr isotopes to reflect melting of metasomatized Precambrian subcontinental lithospheric mantle. The adakitic compositions of the Princeton Group were interpreted by Ickert et al. (2009) to reflect partial melting of basaltic dikes in the lithosphere, with juvenile Nd isotopes indicating no role for Precambrian the subcontinental lithospheric mantle. Breitsprecher et al. (2003), Dostal et al. (2003), and Ickert et al. (2009) suggested that the source of

heat may have been upwelling asthenosphere through a slab window, or slab tear.

Figure 18 shows plots across (longitude) and along (latitude) the volcanic belts. From west to east Ba/La decreases (Fig. 18a); a similar decrease is lacking from south to north (Fig. 18b). The lateral change in Ba/La has been shown to be a good indicator of regional variations across arcs, reflecting declining intensity of fluid flux from the subducting slab (e.g., Patino et al., 2000; Michelfelder et al., 2013). From west to east Sr/Y decreases (Fig. 18c), with the highest values in the Pentiction and Princeton groups. From south to north there is a distinct decrease in Sr/Y (<100) near 50°N (Fig. 18d). Ickert et al. (2009) attributed the high Sr/Y values of the Princeton Group to melting of basaltic dikes in the lithospheric mantle whereas

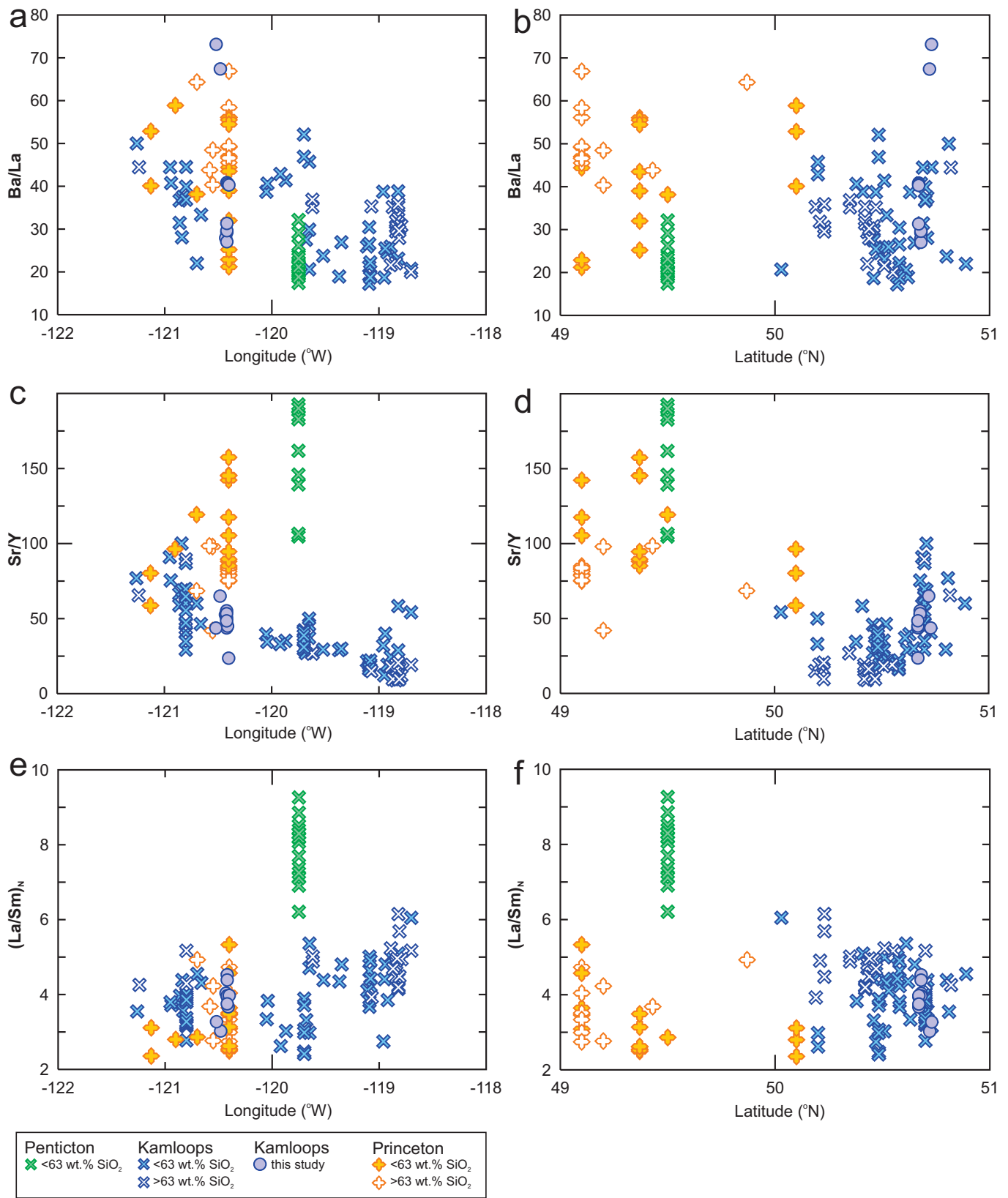


Fig. 18. Latitude and Longitude vs. trace element and REE ratios. **a)** Longitude and **b)** Latitude vs. Ba/La, a proxy for slab-derived fluids (e.g., Patiño et al., 2000; Michelfelder et al., 2013). **c)** Longitude and **d)** Latitude vs. Sr/Y, a proxy for adakitic volcanism (Sr/Y >40). **e)** Longitude and **f)** Latitude vs. chondrite-normalized La/Sm, a proxy for partial melt. Data sources as in Figure 16.

Dostal et al. (2003) suggested that the high Sr values are due to partial melting of a previously metasomatized Precambrian lithosphere. Chondrite-normalized La/Sm increases from west to east (Fig. 18e), but this is controlled in part by more felsic rocks of the Kamloops Group in the east; La/Sm does not decrease from south to north (Fig. 18f). Again, the Penticton Group rocks stand out and are best interpreted as reflecting different source conditions. Forthcoming geochemical data from this study will help to further evaluate these trends and guide future geochemical testing.

5.4. Climatic considerations

The Early Eocene Climatic Optimum (EECO) had a warmer climate than today (Fig. 19; Zachos et al., 2001, 2008; Smith et al., 2010; Hyland et al., 2018; Anagnostou et al., 2020; Inglis et al., 2020; Stokke et al., 2020). The early onset of the EECO is marked by the Paleocene-Eocene thermal maximum (PETM; Fig. 19). Although there is evidence linking volcanism to the onset and termination of the PETM (e.g., Stokke et al., 2020), the relationship of volcanism to the overall EECO remains unclear (e.g., Anagnostou et al., 2020). The Challis-Kamloops belt is but one of a number of regions in the world that witnessed volcanism during the latest Paleocene through early Eocene (e.g., Reagan et al., 2013; Gaina and Jakon, 2019; Stokke et

al., 2020), but the potential contribution to climate fluctuations are unknown. Integrated studies of Kamloops Group volcanism will help constrain the volumes of melt production, duration, and its contribution of volatiles to the Eocene atmosphere.

6. Further work

This preliminary report is part of ongoing larger study of Eocene volcanic rocks in British Columbia. Through detailed physical volcanology, including volcanic architecture and lithofacies relationships, litho-geochemistry, and radiometric age-dating, this project aims to further contribute to the following.

- Re-evaluate and clarify the nomenclature and correlations of volcanic complexes in south-central British Columbia.
- Develop a lateral and stratigraphic context for the volcanic rocks through mapping, geochemistry, and geochronology.
- Test the potential contribution of these volcanic complexes to climate change during the EECO by developing temporal, volume, and volatile flux models.
- Further evaluate the relationship of volcanism to mineralization.

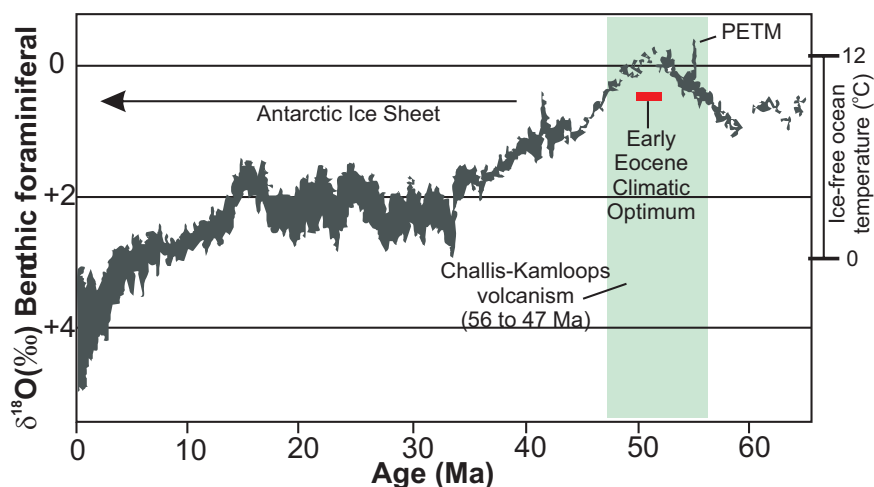


Fig. 19. Age vs. $\delta^{18}\text{O}$ ‰ (Benthic foraminiferal). The $\delta^{18}\text{O}$ ‰ values are a proxy for average sea water temperature, plotted at right, before the growth of the Antarctic ice sheet at ca. 35 Ma. The blue field shows that the Challis-Kamloops belt volcanism overlaps with the Early Eocene Climatic Optimum. PETM – Paleocene-Eocene thermal maximum. Modified from Zachos et al. (2008).

Acknowledgments

We are grateful to Steve Van Wagoner for field assistance and digitizing geologic maps. NVW thanks students in independent studies courses during 2017-18 who participated in studies of Kenna Cartwright Park. G. Jones assisted preparing the geochemistry figures. A review by N. Williamson improved the manuscript.

References cited

Aydınçakır, E., and Sen, C., 2013. Petrogenesis of the post-collisional volcanic rocks from the Borçka (Artvin) area: Implications for the evolution of the Eocene magmatism in the Eastern Pontides (NE Turkey). *Lithos*, 172-173, 98-117. <https://doi.org/10.1016/j.lithos.2013.04.007>.

- Alvarado, G.E., Pérez, W., Vogel, T.A., Gröger, H., and Patiño, L., 2011. The Cerro Chopo basaltic cone (Costa Rica): An unusual completely reversed graded pyroclastic cone with abundant low vesiculated cannonball juvenile fragments. *Journal of Volcanology and Geothermal Research*, 201, 163-177, <https://doi.org/10.1016/j.jvolgeores.2010.11.010>.
- Anagnostou, E., John, E.H., Babila, T.L., Sexton, P.F., Ridgwell, A., Lunt, D.J., Pearson, P.N., Chalk, T.B., Pancost, R.D., and Foster, G.L., 2020. Proxy evidence for state-dependence of climate sensitivity in the Eocene greenhouse. *Nature Communications*, 11, 4436.
- Anderson, S.W., Smrekar, S.E., and Stofan, E.R., 2012. Tumulus development on lava flows: insights from observations of active tumuli and analysis of formation models. *Bulletin of Volcanology*, 74, 931-946.
- Archibald, S.B., Greenwood, D.R., Smith, R.Y., Mathewes, R.W., and Basinger, J.F., 2011. Great Canadian *Lagerstätten* 1. Early Eocene *Lagerstätten* of the Okanagan Highlands (British Columbia and Washington State). *Geoscience Canada*, 38, 155-164.
- Bradshaw, T. K., and Smith, E.I., 1994. Polygenetic Quaternary volcanism at Crater Flat Nevada. *Journal of Volcanology and Geothermal Research*, 63, 165-182.
- Bordet, E., Mihalynuk, M.G., Hart, C.J.R., Mortensen, J.K., Friedman, R.M., and Gabites, J., 2014. Chronostratigraphy of Eocene volcanism, central British Columbia. *Canadian Journal of Earth Sciences*, 51, 56-103, <https://doi.org/10.1139/cjes-2013-0073>.
- Breitsprecher, K., 2002. Volcanic stratigraphy, petrology and tectonic setting of the eastern margin of the Eocene Kamloops Group, south-central British Columbia. Unpublished M.Sc. thesis, Simon Fraser University, 257 p.
- Breitsprecher, K., Thorkelson, D.J., Groome, W.G., and Dostal, J., 2003. Geochemical confirmation of the Kula-Farallon slab window beneath the Pacific Northwest in Eocene time. *Geology*, 31, 351-354, [https://doi.org/10.1130/0091-7613\(2003\)031<0351:GCOTKF>2.0.CO;2](https://doi.org/10.1130/0091-7613(2003)031<0351:GCOTKF>2.0.CO;2).
- Davidson, J., Turner, S., Handley, H., Macpherson, C., and Dosseto, A., 2007. Amphibole 'sponge' in arc crust? *Geology*, 35, 787-790, <https://doi.org/10.1130/G23637A.1>.
- Dostal, J., Church, B.N., Reynolds, P.H., and Hopkinson, L., 2001. Eocene volcanism in the Buck Creek Basin, Central British Columbia (Canada): Transition from arc to extensional volcanism. *Journal of Volcanology and Geothermal Research*, 107, 149-170, [https://doi.org/10.1016/S0377-0273\(00\)00261-4](https://doi.org/10.1016/S0377-0273(00)00261-4).
- Dostal, J., Breitsprecher, K., Church, B.N., Thorkelson, D., and Hamilton, T.S., 2003. Eocene melting of Precambrian lithospheric mantle: Alcaline-bearing volcanic rocks from the Challis-Kamloops belt of south central British Columbia. *Journal of Volcanology and Geothermal Research*, 126, 303-326, [https://doi.org/10.1016/S0377-0273\(03\)00153-7](https://doi.org/10.1016/S0377-0273(03)00153-7).
- Dostal, J., Keppie, J.D., Church, B.N., Reynolds, P.H., and Reid, C.R., 2008. The Eocene-Oligocene magmatic hiatus in the south-central Canadian Cordillera: A capture of the Kula Plate by the Pacific Plate? *Canadian Journal of Earth Sciences*, 45, 69-82, <https://doi.org/10.1139/E07-062>.
- Dostal, J., Keppie, D., and Church, B.N., 2019. Generation of Eocene volcanic rocks from the Cordilleran arc of south-central British Columbia (Canada) during subduction of the Farallon and Resurrection plates and Yellowstone oceanic plateau. *Geological Journal*, 54, 590-604, <https://doi.org/10.1002/gj.3208>.
- Ewing, T.D., 1981a. Geology and tectonic setting of the Kamloops Group, south-central British Columbia. Unpublished Ph.D. thesis, University of British Columbia, 225 p.
- Ewing, T.E., 1981b. Regional stratigraphy and structural setting of the Kamloops Group, south-central British Columbia. *Canadian Journal of Earth Sciences*, 18, 1464-1477, <https://doi.org/10.1139/e81-137>.
- Ewing, T.E., 1981c. Petrology and geochemistry of the Kamloops Group volcanics, British Columbia. *Canadian Journal of Earth Sciences*, 18, 1478-1491, <https://doi.org/10.1139/e81-138>.
- Ewing, T. E., 1982., Geologic map of Tertiary rocks of the Afton-Tranquille area west of Kamloops. British Columbia. British Columbia Ministry of Energy, Mines and Petroleum Resources, British Columbia Geological Survey Preliminary Map 48, 1:50,000 scale.
- Furman, T., and Graham, D., 1999. Erosion of lithospheric mantle beneath the East African Rift system: Geochemical evidence from the Kivu volcanic province. *Developments in Geotectonics*, 24, 237-262, [https://doi.org/10.1016/S0419-0254\(99\)80014-7](https://doi.org/10.1016/S0419-0254(99)80014-7).
- Gaina, C., and Jakob, J., 2019. Global Eocene tectonic unrest: Possible causes and effects around the North American plate. *Tectonophysics*, 760, 136-151, <https://doi.org/10.1016/j.tecto.2018.08.010>.
- Goto, Y., and McPhie, J., 2012. Morphology and formation of spreading cracks on pillow lavas at Cape Grim, northwestern Tasmania, Australia. *Bulletin of Volcanology*, 74, 1611-1619, <https://doi.org/10.1007/s00445-012-0618-9>.
- Greenwood, D.R., Archibald, S.B., Mathewes, R.W., and Moss, P.T., 2005. Fossil biotas from the Okanagan Highlands, southern British Columbia and northeastern Washington State: Climates and ecosystems across an Eocene landscape. *Canadian Journal of Earth Sciences*, 42, 167-185, <https://doi.org/10.1139/e04-100>.
- Greenwood, D.R., Pigg, K.B., and DeVore, M.L., 2016. Eocene paleontology and geology of western north America. *Canadian Journal of Earth Sciences*, 53, 543-547.
- Haeussler, P.J., Bradley, D.C., Wells, R.E., and Miller, M.L., 2003. Life and death of the resurrection plate: Evidence for its existence and subduction in the northeastern Pacific in Paleocene-Eocene time. *Bulletin of the Geological Society of America*, 115, 867-880, [https://doi.org/10.1130/0016-7606\(2003\)115<0867:LADOTR>2.0.CO;2](https://doi.org/10.1130/0016-7606(2003)115<0867:LADOTR>2.0.CO;2).
- Hungerford, J.D.G., Edwards, B.R., Skilling, I.P., and Cameron, B.I., 2014. Evolution of a subglacial basaltic lava flow field: Tennena volcanic center, Mount Edziza volcanic complex, British Columbia, Canada. *Journal of Volcanology and Geothermal Research*, 272, 39-58, <https://doi.org/10.1016/j.jvolgeores.2013.09.012>.
- Hyland, E., Huntington, K.W., Sheldon, N.D., and Reichgelt, T., 2018. Temperature seasonality in the North American continental interior during the Early Eocene Climatic Optimum. *Climate of the Past*, 14, 1391-1404, <https://doi.org/10.5194/cp-14-1391-2018>.
- Ickert, R.B., Thorkelson, D.J., Marshall, D.D., and Ullrich, T.D., 2009. Eocene adakitic volcanism in southern British Columbia: Remelting of arc basalt above a slab window. *Tectonophysics*, 464, 164-185, <https://doi.org/10.1016/j.tecto.2007.10.007>.
- Inglis, G.N., et al., 2020. Global mean surface temperature and climate sensitivity of the early Eocene Climatic Optimum (EECO), Paleocene-Eocene Thermal Maximum (PETM), and latest Paleocene. *Climate of the Past*, 16, 1953-1968.
- Iverson, A.A., Rowe, M.C., Webster, J.D., and Neill, O.K., 2018. Amphibole-, clinopyroxene- and plagioclase-melt partitioning of trace and economic metals in halogen-bearing rhyodacitic melts. *Journal of Petrology*, 59, 1579-1604, <https://doi.org/10.1093/petrology/egy072>.
- Keskin, M., Chugayev, A.V., Lebedev, V.A., and Sharkov, E.V., 2012. The geochronology and origin of mantle sources for late Cenozoic intraplate volcanism in the frontal part of the Arabian plate in the Karacadağ neovolcanic area of Turkey. Part 2. The results of geochemical and isotope (Sr-Nd-Pb) studies. *Journal of Volcanology and Seismology*, 6, 361-382, <https://doi.org/10.1134/S0742046312060048>.

- Krienitz, M.S., Haase, K.M., Mezger, K., Eckardt, V., and Shaikh-Mashail, M.A., 2006. Magma genesis and crustal contamination of continental intraplate lavas in northwestern Syria. *Contributions to Mineralogy and Petrology*, 151, 698-716, <https://doi.org/10.1007/s00410-006-0088-1>.
- Laubier, M., Grove, T.L., and Langmuir, C.H., 2014. Trace element mineral/melt partitioning for basaltic and basaltic andesitic melts: An experimental and laser ICP-MS study with application to the oxidation state of mantle source regions. *Earth and Planetary Science Letters*, 392, 265-278, <https://doi.org/10.1016/j.epsl.2014.01.053>.
- Le Bas, M.J., Le Maitre, R.W., Streckeisen, A., and Zanettin, B., 1986. A chemical classification of volcanic rocks based on the total alkali-silica diagram. *Journal of Petrology*, 27, 745-750.
- Leeman, W.P., Lewis, J.F., Evarts, R.C., Conrey, R.M., and Streck, M.J., 2005. Petrologic constraints on the thermal structure of the Cascades arc. *Journal of Volcanology and Geothermal Research*, 140, 67-105.
- Liang, Y., Liu, X., Qin, C., Li, Y., Chen, J., and Jiang, J., 2017. Petrogenesis of Early Cretaceous mafic dikes in southeastern Jiaolai basin, Jiaodong Peninsula, China. *International Geology Review*, 59, 131-150, <https://doi.org/10.1080/00206814.2016.1213666>.
- Love, D.A., Clark, A.H., Hodgson, C.J., Mortensen, J.K., Archibald, D.A., and Farrar, E., 1998. The timing of adularia-sericite-type mineralization and alunite-kaolinite-type alteration, Mount Skukum epithermal gold deposit, Yukon Territory, Canada; ⁴⁰Ar-³⁹Ar and U-Pb geochronology. *Economic Geology*, 93, 437-462.
- Lowe, A.J., Greenwood, D.R., West, C.K., Galloway, J.M., Sudermann, M., and Reichgelt, T., 2018a. Plant community ecology and climate on an upland volcanic landscape during the Early Eocene Climatic Optimum: McAbee Fossil Beds, British Columbia, Canada. *Palaeogeography, Palaeoclimatology, Palaeoecology*, 511, 433-448, <https://doi.org/10.1016/j.palaeo.2018.09.010>.
- Lowe, A.J., West, C.K., and Greenwood, D.R., 2018b. Volcaniclastic lithostratigraphy and paleoenvironment of the lower Eocene McAbee fossil beds, Kamloops Group, British Columbia, Canada. *Canadian Journal of Earth Sciences*, 55, 923-934.
- MacLean, W.H., and Barrett, T.J., 1993. Lithochemical techniques using immobile elements. *Journal of Geochemical Exploration*, 48, 109-133.
- Madsen, J.K., Thorkelson, D.J., Friedman, R.M., and Marshall, D.D., 2006. Cenozoic to recent plate configurations in the Pacific Basin: Ridge subduction and slab window magmatism in western North America. *Geosphere*, 2, 11-34, <https://doi.org/10.1130/GES00020.1>.
- Maro, G., and Caffè, P.J., 2016. The Cerro Bitiche andesitic field: Petrological diversity and implications for magmatic evolution of mafic volcanic centers from the northern Puna. *Bulletin of Volcanology*, 78, Article 51, <https://doi.org/10.1007/s00445-016-1039-y>.
- Mayr, G., Archibald, S.B., Kaiser, G.W., and Mathewes, R.W., 2019. Early Eocene (Ypresian) birds from the Okanagan Highlands, British Columbia (Canada) and Washington State (USA). *Canadian Journal of Earth Sciences*, 56, 803-813.
- Michelfelder, G.S., Feeley, T.C., Wilder, A.D., and Klemetti, E.W., 2013. Modification of the continental crust by subduction zone magmatism and vice-versa: Across-strike geochemical variations of silicic lavas from individual eruptive centers in the Andean central volcanic zone. *Geosciences*, 3, 633-667, <https://doi.org/10.3390/geosciences3040633>.
- Morris, G.A., and Creaser, R.A., 2003. Crustal recycling during subduction at the Eocene Cordilleran margin of North America: A petrogenetic study from the southwestern Yukon. *Canadian Journal of Earth Sciences*, 40, 1805-1821.
- Patiño, L.C., Carr, M.J., and Feigenson, M.D., 2000. Local and regional variations in Central American arc lavas controlled by variations in subducted sediment input. *Contributions to Mineralogy and Petrology*, 138, 265-283.
- Pearce, J.A., 1996. A user's guide to basalt discrimination diagrams. In: Wyman, D.A., (Ed.), *Trace element geochemistry of volcanic rocks: Applications for massive sulphide exploration*. Geological Association of Canada, Short Course Notes, 12, pp. 79-113.
- Read, P.B., and Hebda, R., 2009. Geological setting and paleontology of the fossiliferous Eocene beds near McAbee, southwestern British Columbia. Online Report, British Columbia Ministry of Agriculture and Lands, 83 p., <https://www2.gov.bc.ca/gov/content/industry/natural-resource-use/fossil-management/mcabee>.
- Reagan, M.K., McClelland, W.C., Girard, G., Goff, K.R., Peate, D.W., Ohara, Y., and Stern, R.J., 2013. The geology of the southern Mariana fore-arc crust: Implications for the scale of Eocene volcanism in the western Pacific. *Earth and Planetary Science Letters*, 380, 41-51, <https://doi.org/10.1016/j.epsl.2013.08.013>.
- Reynolds, P., Brown, R.J., Thordarson, T., Llewellyn, E.W., and Fielding, K., 2015. Rootless cone eruption processes informed by dissected tephra deposits and conduits. *Bulletin of Volcanology*, 77, <https://doi.org/10.1007/s00445-015-0958-3>.
- Ross, P.-S., and Bédard, J.H., 2009. Magmatic affinity of modern and ancient volcanic rocks determined from trace-element discrimination diagrams. *Canadian Journal of Earth Sciences*, 46, 823-839.
- Skilling, I.P., 2002. Basaltic pahoehoe lava-fed deltas: Large-scale characteristics, clast generation, emplacement processes and environmental discrimination. In: Smellie, J.L., and Chapman, M.G., (Eds.), *Volcano-Ice Interaction on Earth and Mars*. Geological Society Special Publication, 202, 91-113, <https://doi.org/10.1144/GSL.SP.2002.202.01.06>.
- Smellie, J.L., Millar, I.L., Rex, D.C., and Butterworth, P.J., 1998. Subaqueous, basaltic lava dome and carapace breccia on King George Island, South Shetland Islands, Antarctica. *Bulletin of Volcanology*, 59, 245-261, <https://doi.org/10.1007/s004450050189>.
- Smith, E.I., Sanchez, A.J., Walker, J.D., and Wang, K., 1999. Geochemistry of mafic magmas in the Hurricane Volcanic Field Utah: Implications for small- and large-scale chemical variability of the lithospheric mantle. *Journal of Geology*, 107, 433-448.
- Smith, R.Y., Greenwood, D.R., and Basinger, J.F., 2010. Estimating paleoatmospheric *p*CO₂ during the Early Eocene Climatic Optimum from stomatal frequency of *Ginkgo*, Okanagan Highlands, British Columbia, Canada. *Palaeogeography, Palaeoclimatology, Palaeoecology*, 293, 120-131.
- Stern, R.J., and Dumitru, T.A., 2019. Eocene initiation of the Cascadia subduction zone: A second example of plume-induced subduction initiation? *Geosphere*, 15, 659-681, <https://doi.org/10.1130/GES02050.1>.
- Stevenson, J.A., Mitchell, N.C., Mochrie, F., Cassidy, M., and Pinkerton, H., 2012. Lava penetrating water: The different behaviours of pāhoehoe and 'a'ā at the Nesjhraun, Þingvellir, Iceland. *Bulletin of Volcanology*, 74, 33-46, <https://doi.org/10.1007/s00445-011-0480-1>.
- Stokke, E.W., Jones, M.T., Tierney, J.E., Svensen, H.H., and Whiteside, J.H., 2020. Temperature changes across the Paleocene-Eocene Thermal Maximum—a new high-resolution TEX₈₆ temperature record from the eastern North Sea Basin. *Earth and Planetary Science Letters*, 544, 116338, <https://doi.org/10.1016/j.epsl.2020.116388>.
- Sun, S.S., and McDonough, W.F., 1989. Chemical and isotopic systematics of oceanic basalts: implications for mantle composition and processes. In: Saunders, A.D., and Norry, M.J., (Eds.), *Magmatism in the Ocean Basins*. Geological Society of London, Special Publication, 42, pp. 313-345.
- Vander Auwera, J., Namur, O., Dutrieux, A., Wilkinson, C.M., Ganerød, M., Coumont, V., and Bolle, O., 2019. Mantle melting and magmatic processes under la Picada stratovolcano (CSVZ,

- Chile). *Journal of Petrology*, 60, 907-944, <https://doi.org/10.1093/petrology/egz020>.
- Van Wagoner, N., and Ootes, L., 2021. Geochemical data from the Kamloops Group (Eocene) volcanic rocks. British Columbia Ministry of Energy, Mines and Low Carbon Innovation, British Columbia Geological Survey GeoFile, in prep.
- Walker, G.P.L., 1992. Morphometric study of pillow-size spectrum among pillow lavas. *Bulletin of Volcanology*, 54, 459-474.
- Walker, J.A., Patiño, L.C., Cameron, B.I., and Carr, M.J., 2000. Petrogenetic insights provided by compositional transects across the Central America arc: southeastern Guatemala and Honduras. *Journal of Geophysical Research*, 105, 18949-18963.
- Walker, J.A., Patiño, L.C., Carr, M.J., and Feigenson, M.D., 2001. Slab control over HFSE depletions in Central Nicaragua. *Earth and Planetary Science Letters*, 192, 533-543, [https://doi.org/10.1016/S0012-821X\(01\)00476-9](https://doi.org/10.1016/S0012-821X(01)00476-9).
- Wang, K., Plank, T., Walker, J.D., and Smith, E.I., 2002. A mantle melting profile across the Basin and Range, SW USA. *Journal of Geophysical Research: Solid Earth*, 107, ECV 5-1-ECV 5-21, <https://doi.org/10.1029/2001jb000209>.
- Wang, J., Xiong, X., Takahashi, E., Zhang, L., Li, L., and Liu, X., 2019. Oxidation state of arc mantle revealed by partitioning of V, Sc, and Ti between mantle minerals and basaltic melts. *Journal of Geophysical Research: Solid Earth*, 124, 4617-4638, <https://doi.org/10.1029/2018JB016731>.
- Wang, X.C., Wilde, S.A., Xu, B., and Pang, C.J., 2016. Origin of arc-like continental basalts: Implications for deep-Earth fluid cycling and tectonic discrimination. *Lithos*, 261, 5-45, <https://doi.org/10.1016/j.lithos.2015.12.014>.
- West, C.K., Greenwood, D.R., Reichgelt, T., Lowe, A.J., Vachon, J.M., and Basinger, J.F., 2020. Paleobotanical proxies for early Eocene climates and ecosystems in northern North America from middle to high latitudes. *Climate of the Past*, 16, 1387-1410.
- Winchester, J.A., and Floyd, P., 1977. Geochemical discrimination of different magma series and their differentiation products using immobile elements. *Chemical Geology*, 20, 325-343.
- Woodhead, J.D., Hergt, J.M., Davidson, J.P., and Eggins, S.M., 2001. Hafnium isotope evidence for 'conservative' element mobility during subduction zone processes. *Earth and Planetary Science Letters*, 192, 331-346, [https://doi.org/10.1016/S0012-821X\(01\)00453-8](https://doi.org/10.1016/S0012-821X(01)00453-8).
- Yamagishi, H., 1987. Studies on the Neogene subaqueous lavas and hyaloclastites in southwest Hokkaido. Report of the Geological Survey of Hokkaido, No. 59, 55-117.
- Yamagishi, H., 1991. Morphological and sedimentological characteristics of the Neogene submarine coherent lavas and hyaloclastites in Southwest Hokkaido, Japan. *Sedimentary Geology*, 74, 5-23, [https://doi.org/10.1016/0037-0738\(91\)90032-9](https://doi.org/10.1016/0037-0738(91)90032-9).
- Zachos, J., Pagani, H., Sloan, L., Thomas, E., and Billups, K., 2001. Trends, rhythms, and aberrations in global climate 65 Ma to present. *Science*, 292, 686-693, <https://doi.org/10.1126/science.1059412>.
- Zachos, J.C., Dickens, G.R., and Zeebe, R.E., 2008. An early Cenozoic perspective on greenhouse warming and carbon-cycle dynamics. *Nature*, 451, 279-283, <https://doi.org/10.1038/nature06588>.
- Zhang, L., Li, S., and Zhao, Q., 2019. A review of research on adakites. *International Geology Review*, doi:10.1080/00206814.2019.1702592.
- Zhang, J., Liao, M., Santosh, M., Yang, Z., Zhang, Y., and Dai, Y., 2020. Middle Tonian calc-alkaline picrites, basalts, and basaltic andesites from the Jiangnan Orogen: Evidence for rear-arc magmatism. *Precambrian Research*, 350, 105943, <https://doi.org/10.1016/j.precamres.2020.105943>.